Diverse communities of Bacteria and Archaea flourished in Palaeoarchaean (3.5-3.3 Ga) microbial mats

DIVERSE COMMUNITIES OF BACTERIA AND ARCHAEA FLOURISHED IN PALAEOARCHAEAN (3.5–3.3 GA) MICROBIAL MATS

by KEYRON HICKMAN-LEWIS[1,2] FRANCES WESTALL[2] *and* BARBARA CAVALAZZI[1,3]

[1]Dipartimento Biologiche, Geologiche e Ambientali, Università di Bologna, via Zamboni 67, I-40126, Bologna, Italy; keyron.hickman-lewis@cnrs-orleans.fr
[2]CNRS Centre de Biophysique Moléculaire, Rue Charles Sadron, 45071, Orléans, France
[3]and Park, 2006, Johannesburg, South Africa

Abstract: Limited taxonomic classification is possible for Archaean microbial mats and this is a fundamental limitation in constraining early ecosystems. Applying Fourier transform infrared spectroscopy (FTIR), a powerful tool for identifying vibrational motions attributable to specific functional groups, we characterized fossilized biopolymers in 3.5–3.3 Ga microbial mats from the Barberton greenstone belt (South Africa). Microbial mats from four Palaeoarchaean horizons exhibit significant differences in taxonomically informative aliphatic contents, despite high aromaticity. This reflects precursor biological heterogeneity since all horizons show equally exceptional preservation and underwent similar grades of metamorphism. Low methylene to end-methyl (CH_2/CH_3) absorbance ratios in mats from the 3.472 Ga Middle Marker horizon signify short, highly branched *n*-alkanes interpreted as isoprenoid chains forming archaeal membranes. Mats from the 3.45 Ga Hooggenoeg Chert H5c, 3.334 Ga Footbridge Chert, and 3.33 Ga Josefsdal Chert exhibit higher CH_2/CH_3 ratios suggesting mostly longer, unbranched fatty acids from bacterial lipid precursors. Absorbance ratios of end-methyl to methylene (CH_3/CH_2) in Hooggenoeg, Josefsdal and Footbridge mats yield a range of values (0.20–0.80) suggesting mixed bacterial and archaeal architect communities based on comparison with modern examples. Higher (0.78–1.25) CH_3/CH_2 ratios in the Middle Marker mats identify Archaea. This exceptional preservation reflects early, rapid silicification preventing the alteration of biogeochemical signals inherited from biomass. Since silicification commenced during the lifetime of the microbial mat, FTIR signals estimate the affinities of the architect community and may be used in the reconstruction of Archaean ecosystems. Together, these results show that Bacteria and Archaea flourished together in Earth's earliest ecosystems.

Key words: Precambrian, Barberton greenstone belt, infrared spectroscopy, microbial mat, geobiology, biosignature.

Palaeoarchaean microbial mats preserved in chert are the oldest and most robust evidence for life on Earth. The biological affinities and metabolisms of their architect organisms are, however, subject to enduring debate (Nisbet & Fowler 1999; Tice & Lowe 2006; Bosak *et al.* 2007, 2010). They are assumed to have been anoxygenic and photosynthetic (Tice & Lowe 2006; Tice 2009; Noffke 2010; Noffke *et al.* 2013; Westall *et al.* 2011; Homann *et al.* 2015, 2018; Trower & Lowe 2016; Hickman-Lewis *et al.* 2018*a*) but their phylogenetic placement and most aspects of their palaeobiology remain unconstrained because the Archaean fossil record is altered by processes of maturation and metamorphism, at times susceptible to ambiguity in interpretation, and lacks modern environmental analogues. This lack of biological specificity is a fundamental limitation for constraining the nature of the earliest ecosystems. In this contribution, we study taxonomically indicative signals using transmission Fourier transform infrared spectroscopy (FTIR) analyses of multiple microbial mat horizons (*c.* 3.47–3.33 Ga; Figs 1, 2) from the Barberton greenstone belt, southern Africa. We evaluate statistically significant differences in the compositions of these carbonaceous microbial horizons to distinguish aliphatic (and aromatic) groups indicative of precursor biomolecules that provide information about the biological affinities of the architect microbial communities. The objective of this study is, for the first time, to place unambiguous taxonomic and

phylogenetic constraints on the organisms inhabiting Earth's earliest ecosystems. Our finding that microbial mats in Palaeoarchaean rocks preserve spectral vestiges of their diverse architect communities represents a major step toward reconstructing the ecologies of the earliest ecosystems and the metabolic networks that regulated Archaean biogeochemical cycling.

FTIR as a tool for palaeobiological characterization

FTIR is a vibrational spectroscopy technique that irradiates samples with polychromatic IR light and quantifies changes in dipole moment during molecular vibrational motion (e.g. stretching, bending and rotating). The absorption of IR light during these motions allows the

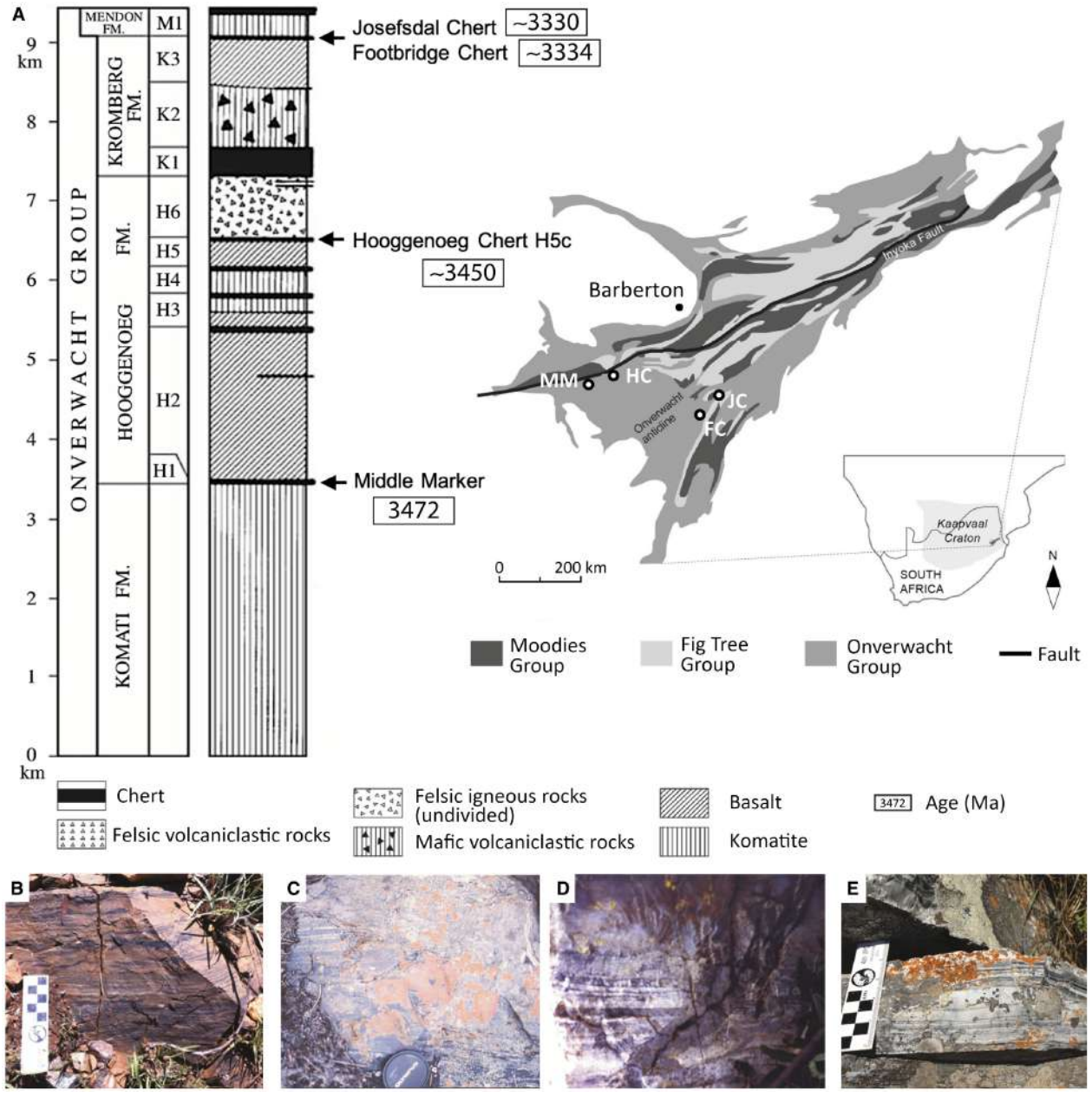

FIG. 1. A, generalized stratigraphic column of the ~3.5–3.3 Ga Onverwacht Group, Barberton greenstone belt, indicating the position of the four studied horizons: the Middle Marker horizon (MM), Hooggenoeg Chert H5c (HC), Footbridge Chert (FC) and Josefsdal Chert (JC); inset shows sampling localities within the context of the Barberton greenstone belt and Kaapvaal craton; adapted from Byerly *et al.* (2018) and Homann *et al.* (2015). B, Middle Marker horizon outcrop (samples MM1 and MM2). C, Hooggenoeg Formation H5c chert outcrop (samples HC1 and HC2). D, Footbridge Chert outcrop (sample FC1). E, Josefsdal Chert outcrop (samples JC1 and JC2). Scale bars in cm; lens cap approx. 50 mm wide. Colour online.

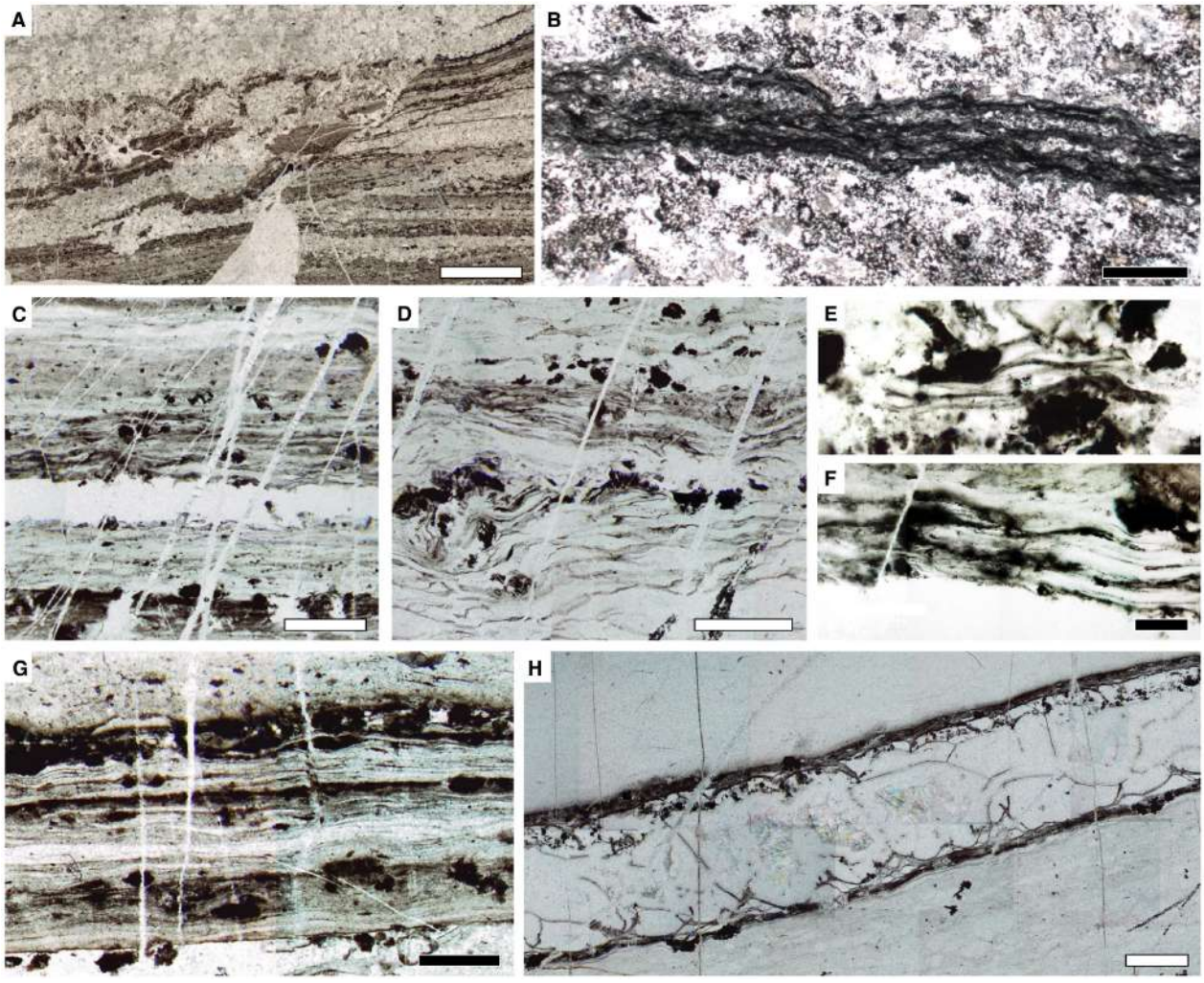

FIG. 2. Petrographic characterization of microbial mat horizons in Palaeoarchaean biolaminites. A–B, Middle Marker horizon; A, MM2; B, MM1. C–F, Hooggenoeg Formation H5c chert: C, E, HC1; D, F, HC2. G, Footbridge Chert; FC1. H, Josefsdal Chert; JC1. Mats exhibit deformation fabrics resulting from the *in vivo* plasticity of EPS-bound microbial mats and are preserved in three dimensions, a testament to the rapidity of their silicification. Scale bars represent: 4 mm (A); 1 mm (B); 300 μm (C, D, G, H); 50 μm (E, F). Colour online.

identification of atomic bonding in such chemical species as molecules, functional groups and cation–anion pairs (Benning *et al.* 2004; Chen *et al.* 2015; Olcott Marshall & Marshall 2015). Among the most powerful uses of FTIR is its ability to characterize cell compounds and structures, thereby taxonomically differentiating organisms according to their dominant biomolecules (Naumann *et al.* 1991, 1996; Helm & Naumann 1995; Choo-Smith *et al.* 2001). Bacteria and Archaea, the two domains of life relevant to deep time palaeobiology, have strikingly different cell envelope compositions: bacterial membrane lipids are composed of ester lipids (e.g. fatty acids), whereas archaeal lipids are composed of ether lipids (e.g. isoprenoids) (Atlas 1989; Albers & Meyer 2011). These chemical differences are identifiable by FTIR, as are other features characteristic of either of these domains, for instance the proteinaceous S-layer and glycosylated extracellular proteins that are associated with Archaea (Helm & Naumann 1995; Igisu *et al.* 2012).

In light of these potentials, FTIR has been demonstrated as an effective means for non-destructive chemical characterization of Phanerozoic organic materials (Gupta *et al.* 2007; Steemans *et al.* 2010; Fraser *et al.* 2012; Hackley *et al.* 2017) and Precambrian organic microfossils (Marshall *et al.* 2005; Igisu *et al.* 2006, 2009, 2018; Javaux & Marshall 2006; Qu *et al.* 2015). Reviews of the application of FTIR to geological and palaeontological specimens are given in Chen *et al.* (2015) and Olcott Marshall & Marshall (2015). Transmission FTIR on thin sections (e.g. Igisu *et al.* 2009, 2018; this study) is an *in situ* IR

approach that mitigates the potential contamination by volatile hydrocarbons in laboratory air inherent to studies of powdered samples (e.g. Derenne *et al.* 2008). In micropalaeontological specimens, comparison with published spectral libraries may be used to identify, for example, functional groups attached to the molecular framework of carbonaceous materials (Bellamy 1954; Socrates 1980; Painter *et al.* 1985; Lin & Ritz 1993; Marshall *et al.* 2005; Igisu *et al.* 2009; Steemans *et al.* 2010). IR spectroscopy is generally applied to minimally altered materials of low thermal maturity (Arouri *et al.* 1999; Marshall *et al.* 2005; Steemans *et al.* 2010; Olcott Marshall & Marshall 2015; Hackley *et al.* 2017), however, studies on older palaeontological materials of higher metamorphic grade (Igisu *et al.* 2006, 2009, 2018) have also yielded informative palaeobiological datasets unavailable through other vibrational spectroscopy approaches.

Most FTIR vibrations of relevance to biology are the organic spectral features occurring within the mid-IR region between wavenumbers 700 and 4000 cm^{-1} (Bellamy 1954; Socrates 1980; Painter *et al.* 1985; Helm & Naumann 1995; Naumann *et al.* 1996). This range includes aromatic, aliphatic, hydroxyl, carboxyl and carbonyl functional groups, as well as amides, polysaccharides and nucleic acids. Regions of particular interest include the aliphatic stretching region between 2800 and 3050 cm^{-1}, and the aromatic-alkenic-carbonyl region between 700 and 1800 cm^{-1}, which contains information on both biological compounds and their interactions with mineral substrates, including silicates and carbonates (Benning *et al.* 2004; Yee *et al.* 2004; Igisu *et al.* 2009, 2018; Guido *et al.* 2013).

Membrane lipid composition distinguishes biological domains

The CH_2/CH_3 ratio (Eqn 1; Lin & Ritz 1993) provides both an estimation of the length of aliphatic chains and a branching index such that an increase in the CH_2/CH_3 ratio indicates longer or less branched aliphatic chains. Marshall *et al.* (2005) used this ratio to approximate different *n*-alkane chain lengths in Meso-Neoproterozoic acritarchs, thus quantifying structural variation in their membrane biopolymers. Steemans *et al.* (2010) later used the ratio to make taxonomic distinctions between Silurian miospores. Herein, we use the CH_2/CH_3 ratio to deduce the *n*-alkane chain length of preserved biopolymers in microbial mat material. It has been demonstrated that differences in the absorbance (Abs) ratio of aliphatic CH_3 and CH_2 moieties after linear baseline correction, i.e. the CH_2/CH_3 and CH_3/CH_2 ratios (Eqns 1, 2) highlighted in Lin & Ritz (1993), Marshall *et al.* (2005) and Igisu *et al.* (2006, 2009, 2012, 2018), can distinguish the nature of precursor membrane lipids. As noted above, the composition of membrane lipids is considered the most fundamental distinction between extant Archaea and Bacteria (Albers & Meyer 2011).

$$\frac{CH_2}{CH_3} = \frac{Abs_{CH_2}}{Abs_{CH_3}} = \frac{Abs_{\sim 2925\ cm^{-1}}}{Abs_{\sim 2960\ cm^{-1}}} \quad (1)$$

$$\frac{CH_3}{CH_2} = R_{3/2} = \frac{Abs_{CH_3}}{Abs_{CH_2}} = \frac{Abs_{\sim 2960\ cm^{-1}}}{Abs_{\sim 2925\ cm^{-1}}} \quad (2)$$

In terms of FTIR spectral distinctions of CH_2 and CH_3, archaeal lipids are composed of mostly highly branched isoprenoid chains with higher $R_{3/2}$ absorbance ratios, whereas bacterial lipids consist of longer, straighter, fatty acid-like hydrocarbons with lower aliphatic $R_{3/2}$ ratios (Atlas 1989; Igisu *et al.* 2009). Igisu *et al.* (2009, 2012) validated the logic of this approach. Igisu *et al.* (2009) demonstrated a similarity in $R_{3/2}$ ratios between fossil and extant cyanobacteria (*Synechocystis* sp. PCC6803) and suggested that the CH_3/CH_2 ratio of membrane lipids usually controls the CH_3/CH_2 ratio of the whole cell. Igisu *et al.* (2012) used cultured Bacteria and Archaea to prove that the $R_{3/2}$ ratio varies between the two domains, and between cellular components. This approach has been applied to distinguishing fossilized organisms, for instance by demonstrating that the $R_{3/2}$ values of microfossils from the 1.88 Ga Gunflint Formation (including *Gunflintia* spp. and *Huroniospora*) and the 850 Ma Bitter Springs Formation (including *Cephalophytarion* and *Glenobotryoidion*) are consistent with a bacterial affinity (Igisu *et al.* 2009), corroborating their palaeobiological determination as cyanobacteria (Barghoorn & Tyler 1965; Schopf & Blacic 1971; Awramik & Barghoorn 1977).

FTIR spectra change little with maturation and metamorphism

Experimental approaches have demonstrated that FTIR spectra evolve during maturation and metamorphism, primarily through the addition of heat (Fraser *et al.* 2014; Jardine *et al.* 2015); however, well-preserved biomolecules have been identified in identical extant and extinct species (Fraser *et al.* 2012; Hackley *et al.* 2017). Generally, the peak intensities of aliphatic bands are observed to reduce in magnitude, whereas aromatic bands show limited relative change (Fraser *et al.* 2014; Jardine *et al.* 2015). Consequently, the ratio of the intensity of the aliphatic C–H stretching region (2800–3050 cm^{-1}) to that of the aromatic ring stretch (~1600 cm^{-1}) reflects the degree of aromaticity of the carbonaceous material (Eqn 3), which generally increases with metamorphic grade. Thus, Archaean microfossils subjected to lower greenschist metamorphism are largely composed of aromatic carbonaceous materials. This

can be compared with Raman spectral characteristics, particularly the relative intensities of the D and G-bands, which denote the thermal maturity (i.e. syngenicity) of carbonaceous materials and the nature of their non-polar aromatic frameworks. Raman spectroscopy of Palaeoarchaean carbonaceous materials suggests that they are composed of heterogeneous, but generally poorly ordered, weakly graphitized, mixed sp^2 and sp^3 carbon (Marshall *et al.* 2007, 2010). Relics of other carbon-bearing groups, for example amides, carbonyl (C=O) and carboxyl (R–COOH) groups, may be also present in fossilized carbonaceous materials (Steemans *et al.* 2010; Jardine *et al.* 2015). The relative proportions of carbon-bearing groups are assessed using the following three equations:

$$\frac{\text{Aliphatic}}{\text{Aromatic}} = \frac{\text{Abs}_{\text{al}}}{\text{Abs}_{\text{ar}}} = \frac{\text{Abs}_{3000-2800\ \text{cm}^{-1}}}{\text{Abs}_{1600\ \text{cm}^{-1}}} \quad (3)$$

$$\frac{\text{Aliphatic}}{\text{Carbonyl}} = \frac{\text{Abs}_{2925\ \text{cm}^{-1}}}{\text{Abs}_{1710\ \text{cm}^{-1}}} \quad (4)$$

$$\frac{\text{Carbonyl}}{\text{Aromatic}} = \frac{\text{Abs}_{1710\ \text{cm}^{-1}}}{\text{Abs}_{1600\ \text{cm}^{-1}}} \quad (5)$$

Since organic matter has a tendency to remain stable during diagenesis due to the insolubility of the lipid fraction in water (Peters *et al.* 2005), low-maturity organic materials have the potential to preserve IR spectral characteristics diagnostic of the precursor material (Igisu *et al.* 2009; Guido *et al.* 2012; Olcott Marshall & Marshall 2015) even through low-grade metamorphism (Igisu *et al.* 2018). Naturally matured kerogens have been shown to undergo only a small initial change in aliphatic compositions due to scission of the C–C bond adjacent to aromatic moieties (Lin & Ritz 1993; Lis *et al.* 2005; Igisu *et al.* 2009). This chain shortening can, nonetheless, be compensated by simultaneous breakage of a C–C bond next to a tertiary carbon atom (Lis *et al.* 2005). Thus, the aliphatic chemistry accessible through FTIR analyses may undergo no measurable change during diagenesis. Increasing metamorphic alteration (subgreenschist facies) nonetheless leads to muting (i.e. decreased intensity) of the FTIR peaks associated with biological materials (Guido *et al.* 2013; Igisu *et al.* 2018).

MATERIAL AND METHOD

Sampling and fundamental characterization

Samples were collected during field campaigns to the Barberton greenstone belt between 2003 and 2012 and all sampling locations may be re-located by means of their global positioning system (GPS) co-ordinates. All samples are stored at the Lithothèque of the CNRS Centre de Biophysique Moléculaire, Orléans, France. Samples of banded, carbonaceous, microbial mat-rich cherts were obtained from the 3.472 Ga Middle Marker horizon, 3.45 Ga Hooggenoeg Formation H5c chert, 3.334 Ga Footbridge Chert and ~3.33 Ga Josefsdal Chert (Figs 1, 2). The petrography and microbial fossils in these cherts are described in detail elsewhere (Walsh & Lowe 1999; Westall *et al.* 2011, 2015; Hickman-Lewis *et al.* 2018*a*, *b*, 2020*a*).

The palaeoenvironmental settings of these four horizons were addressed in detail by Hickman-Lewis *et al.* (2020*a*), who used a combination of bulk ICP-MS and *in situ* laser ablation ICP-MS to determine that these microbial mats flourished under complex aqueous regimes resulting from the confluence of anoxic marine, hydrothermal and terrigenous (riverine) contributions. It was found that the Hooggenoeg and Josefsdal mats grew in conditions relatively more influenced by marine and hydrothermal activity than the Middle Marker and Footbridge mats. Trace and rare earth element geochemistry showed that the mats flourished in variably restricted coastal basins with strong continental influences from mixed ultramafic, mafic and felsic sources, which presumably provided essential nutrients, particularly transition metals, to sustain mat growth (Hickman-Lewis *et al.* 2020*a*). The microbial mats themselves have been interpreted as originating from anoxygenic photosynthetic microbes due to their occurrence in anoxic shallow-water sedimentary successions (Walsh & Lowe 1999; Westall *et al.* 2011, 2015; Hickman-Lewis *et al.* 2018*a*, *b*, 2020*a*).

Previously reported Raman spectra of these microbial mats show bands at ~1350 and ~1600 cm^{-1}, corresponding to disordered and graphitic carbonaceous material; i.e. poorly ordered, randomly layered, polyaromatic domains that have undergone metamorphic temperatures of 285–400°C (e.g. Xie *et al.* 1997; Tice *et al.* 2004; Westall *et al.* 2011, 2015; Hickman-Lewis *et al.* 2018*a*, 2020*b*). We will not focus further on these Raman spectra in this contribution. It suffices to say that this characterization demonstrates that, while this carbonaceous material has undergone some degree of maturation, it has not been completely graphitized; thus, based upon well-constrained experimental work, it is plausible to identify C–H and other bonds within its structure (Fraser *et al.* 2014; Jardine *et al.* 2015).

Transmission Fourier transform infrared spectroscopy

Transmission FTIR was performed on microbial mats from the above-mentioned Middle Marker horizon,

Hooggenoeg Chert H5c, Footbridge Chert and Josefsdal Chert. Representative microbial fabrics are detailed in the photomicrographs shown in Figure 2. Optical microscopy was used both to identify mat fabrics in thin section and to confirm that all regions of interest were free from oxidative weathering, percolative chemical alteration or post-diagenetic remineralization that may influence FTIR spectra (see Jardine *et al.* 2015). Samples were prepared as detached doubly polished thin sections, which were removed from their glass slides by dissolution of cyanoacrylate adhesive. High-magnification optical microscopy was again used after detachment to confirm that all adhesive had been removed from the regions of analysis.

FTIR measurements were conducted at the Centro Interdipartimentale Grandi Strumenti (Università degli studi di Modena e Reggio Emilia, Modena, Italy) using a Bruker VERTEX 70 instrument equipped with a GLOBAR (silicon carbide) source and a deuterated triglycine sulphate (DTGS) detector with a KBr window. Several microbial mats were analysed within each detached section and multiple regions of interest (between 4 and 20) were measured within each mat. Representative complete spectra are shown in Figure 3. Each reported FTIR spectrum is an average of 16 spectra accumulated within the studied area (<1 mm^2; i.e. completely within the microbial mat horizon) within a spectral range of 7500–370 cm^{-1} with a 4 cm^{-1} spectral resolution. Therefore, between 64 and 320 spectra were obtained for each sample. A reference background spectrum in air (T_{bkg}) was taken before each analysis and subtracted from the sample spectrum to remove environmental noise from the signal. FTIR spectra for samples (T_{sample}) are reported as absorbance (Abs = $\log_{10}$[1/transmittance]) relative to the reference (absorbance = $\log_{10}[T_{sample}/T_{bkg}]$). All spectra presented are reported as absorbance versus wavenumber (cm^{-1}). To derive characteristic frequencies and compare relative intensities, the studied regions of each background-corrected spectra were baseline-corrected. The baseline correction was applied as a two-point straight line between two end-points of the desired frequency region according to the methods of Benning *et al.* (2004), Marshall *et al.* (2005) and Igisu *et al.* (2006, 2009, 2018). First-order derivative spectra were calculated to identify any spectral features occluded by adjacent or overlapping peaks (Fraser *et al.* 2012).

Systematic band identifications were made in spectral regions crucial for determining the composition of carbonaceous material (Figs 4–7). Peak identification took into consideration the variable wavenumbers associated with similar or identical features in previous publications, e.g. wavenumbers between 2920 and 2930 cm^{-1} have been attributed to the antisymmetric methylene CH_2 stretch (Bellamy 1954). Peak identifications are indicated in Figure 4 for the aliphatic region and Figure 5A for the aromatic-alkenic region. Increasing maturity can lead to changes in peak position, for example, aromatization of lipids leads to the movement of their diagnostic peaks to lower frequencies (Benning *et al.* 2004; Fraser *et al.* 2014; Jardine *et al.* 2015). Given the often highly controversial nature of suggesting biomolecular complexity in traces of ancient life, we have identified IR bands as corresponding to specific molecular features only where no plausible alternatives (such as matrix mineralogy) exist, following listings in Bellamy (1954), Socrates (1980), Painter *et al.* (1985), Benning *et al.* (2004), Yee *et al.* (2004), Marshall *et al.* (2005), Chen *et al.* (2015) and Igisu *et al.* (2009, 2018). Numerous peaks within the 1400–2000 cm^{-1} range are interpreted as Si–O (Igisu *et al.* 2009; Fig. 6B) therefore, although first-order derivative spectra enable the distinction of certain peaks in this region (Fig. 6), identifications were made in a highly conservative fashion.

Spectra were also obtained for the cyanoacrylate adhesive, finding major absorption bands at 2988, 2944, 2908, and 2876 cm^{-1} within the aliphatic C–H stretching region and weak bands at 1450 and 1375 cm^{-1} (Fig. 7H), consistent with cautions raised by Igisu *et al.* (2009).

All FTIR data for this study are available in Hickman-Lewis *et al.* (2020*c*).

RESULTS

3.472 Ga Middle Marker horizon

Crinkly microbial laminations exhibiting local microtufted morphologies were analysed in two samples, MM1 and MM2 (07SA21 and 07SA23 in the Orléans Lithothèque classification), representative photomicrographs of which are shown in Figure 2A–B. In the aliphatic C–H stretching region (2800–3050 cm^{-1}; Fig. 4A), both samples exhibit bands at 2960 cm^{-1} (asymmetrical

FIG. 3. Representative selections of transmission Fourier transform infrared (FTIR) absorbance spectra in the range 500–4000 cm^{-1}. A, Middle Marker horizon sample MM2. B, Hooggeoneg Formation H5c sample HC1. C, Footbridge Chert sample FC1. D, Josefsdal Chert sample JC1; highlighted zones are relevant to the composition of the aromatic and aliphatic moieties in carbonaceous materials (after Socrates, 1980; Painter *et al.* 1985; Marshall *et al.* 2005; Igisu *et al.* 2009; Guido *et al.* 2013; Chen *et al.* 2015). The region around 2300 cm^{-1} is discounted from discussion, since it results from ambient CO_2.

A
absorbance
B
absorbance
C
absorbance
D
absorbance
O-H
aromatic stretching
aliphatic C-H stretching
aromatic stretching
aromatic stretching
3900
3700
3500
3300
3100
2900
2700
2500
2300
2100
1900
1700
1500
1300
1100
900
700
wavenumber (cm−1)

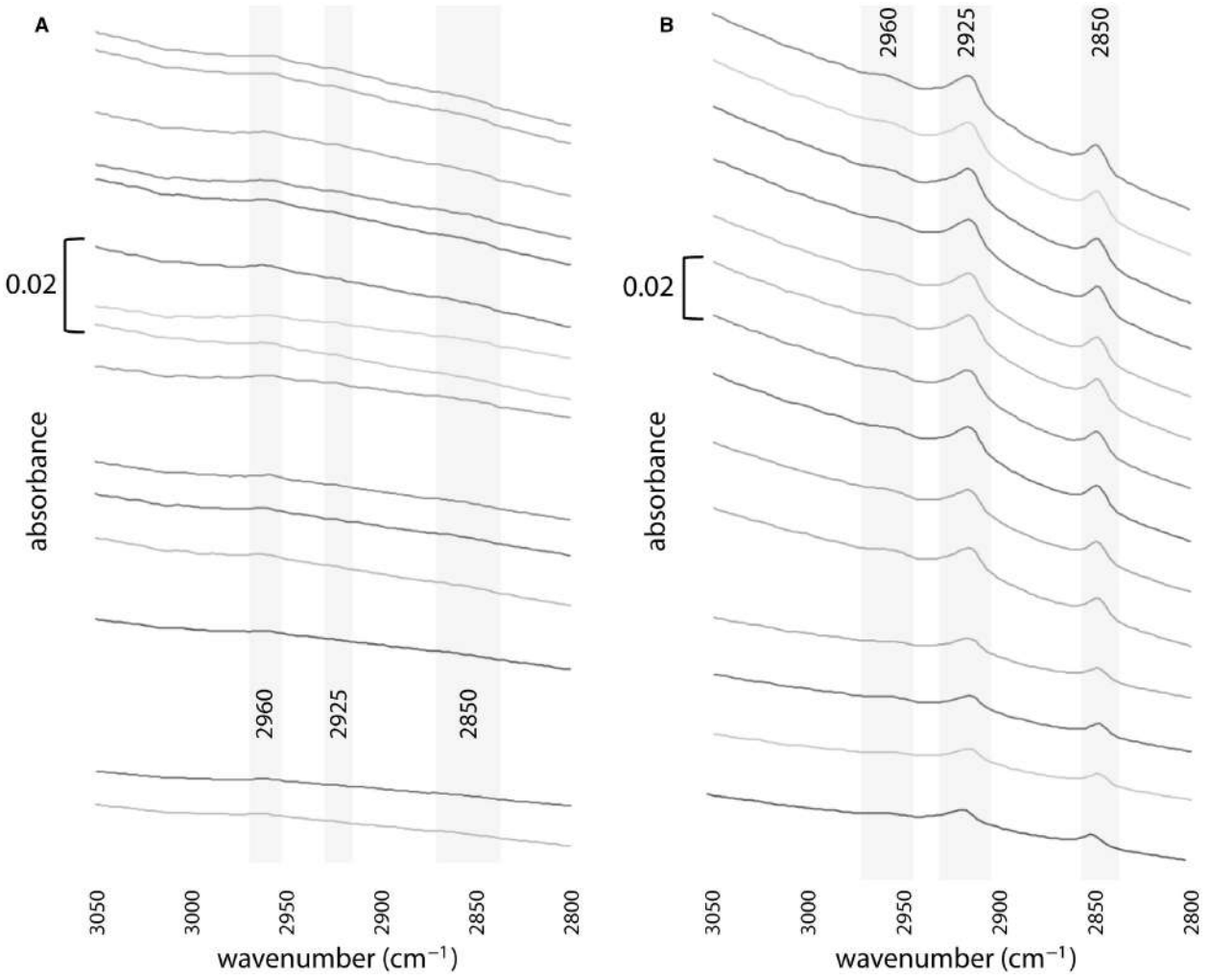

FIG. 4. Representative transmission Fourier transform infrared (FTIR) absorbance spectra in the range 2800–3050 cm^{-1}. A, Middle Marker horizon sample MM1. B, Hooggenoeg Formation H5c sample HC2. C, Footbridge Chert sample Fc1. D, Josefsdal Chert sample JC1.

end-methyl CH_3 stretching), and weak peaks at 2920–2925 cm^{-1} (asymmetrical methylene CH_2 stretching) and 2850 cm^{-1} (symmetrical CH_2 stretching). Sample MM2 shows a further broad, high-intensity band at 2870–2875 cm^{-1}, i.e. symmetrical CH_3 stretching. Although this band may be interpreted to result from the adhesive (Fig. 7H), the absence of bands at 2944 and 2908 cm^{-1}, in addition to the ubiquitous presence of the band at 2960 cm^{-1}, lead us to attribute the band at 2870–2875 cm^{-1} to an indigenous CH_3 component.

In the aromatic/alkenic region (~1300–1800 cm^{-1}; Fig. 5A) sample MM1 exhibits weak bands at 1338 and 1360 cm^{-1} that are also attributable to CH_3 and an intense band at 1456 cm^{-1} assigned to asymmetrical CH_2 stretching. Bands at 1444 and 1464 cm^{-1} are attributed to C–H stretching with a contribution from aromatic ring stretching. The bands at 1394, 1415 and 1728–1743 cm^{-1} are assigned to the symmetrical stretch of C–O, COO and the >C=O ester stretch, respectively, of carboxyl groups. A distinct feature at 1473 cm^{-1} and a shoulder at 1770–1778 cm^{-1} are both attributed to ester C=O, while bands at 1633–1651 cm^{-1} indicate highly conjugated C=O. A weak feature around 1537 cm^{-1} may reflect aliphatic COOH. Olefinic and aromatic groups, together with contributions from carboxyl COOH account for the peaks at 1554, 1568 and 1574 cm^{-1}. Furthermore, carbonyl C=O and carboxyl COOH (1689 and 1703 cm^{-1}) are superposed onto the Si–O peak 1682 cm^{-1}. Carbonyl and carboxyl groups also account for well-defined bands on the shoulder of this peak at 1710 and 1720 cm^{-1}. Further weak shoulders to this Si–O peak at 1666 and 1672 cm^{-1} probably result from alkyl and/or phenyl groups. Bands at 1487 and 1493 cm^{-1} correspond to aromatic ring stretches with a contribution from Si–O, and the bands at 1504 and 1600 cm^{-1}, the latter particularly prominent, are

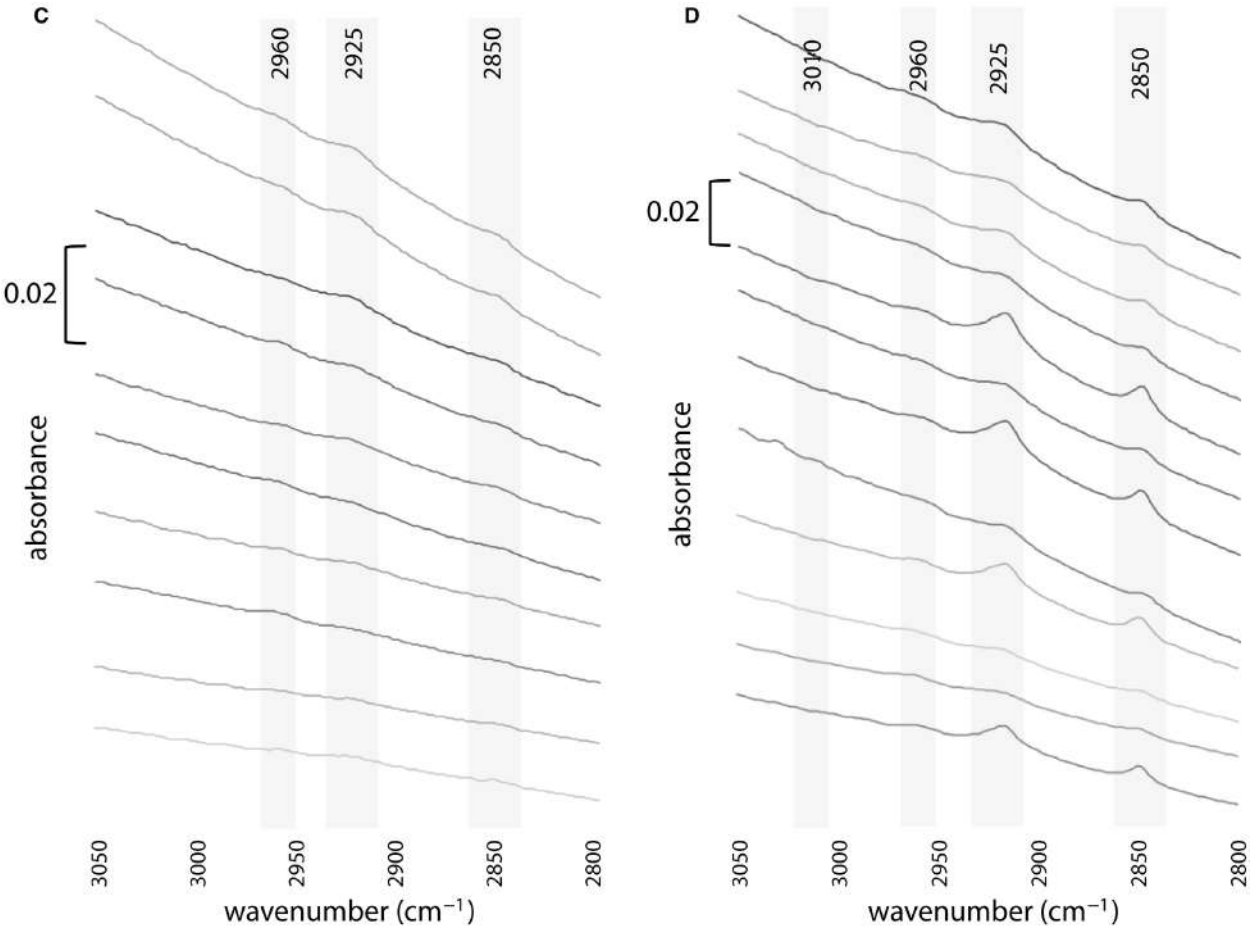

FIG. 4. (Continued)

attributed to aromatic ring stretching (C=C). Finally, a weak shoulder on the 1600 cm^{-1} C=C band at 1618 cm^{-1} may be δNH. Other peaks within the 1400–2000 cm^{-1} range at 1514–1527 and 1790–1792 cm^{-1} are interpreted as Si–O after Igisu *et al.* (2009). It should be noted that the FTIR absorption intensity of samples from the Middle Marker is one order of magnitude lower than in the other samples analysed.

Sample MM2 exhibits additional peaks at 1373 cm^{-1}, attributed to CH_3, at 1430 cm^{-1}, also attributed to aliphatic C–H stretching, and at 1732 cm^{-1}, attributed to the >C=O ester stretch. These spectra do not exhibit the bands at 1568 cm^{-1} and 1770 cm^{-1} indicating lower contributions from C=O. The ester C=O moves to a lower wavenumber (1469 cm^{-1}), whereas the weak δNH feature on the 1600 cm^{-1} C=C band moves to a higher wavenumber (1622 cm^{-1}). All other peak identifications remain the same as in MM1.

3.45 Ga Hooggenoeg Chert H5c

Two sequences of microbial laminations from the same outcrop of Hooggenoeg Formation unit H5c were studied: HC1, containing flat-laminated biofilm sequences several millimetres in thickness; and HC2, in which the laminations are undulatory (representative examples in Fig. 2C–F) (03SA15 and 03SA15B in the Orléans Lithothèque). Both samples show absorption bands in the aliphatic C–H stretching region at 2850, 2920 and 2960 cm^{-1} (spectra of HC2 given in Fig. 4B) attributed to symmetrical and asymmetrical CH_2 and CH_3 stretching as detailed above. Some spectra in HC2 also show a very weak feature at 2870–2875 cm^{-1} corresponding to the symmetrical CH_3 stretch. In spectra from HC1, the broad feature centred on 2925 cm^{-1} probably incorporates a minor contribution from the band at 2890 cm^{-1} (C–H

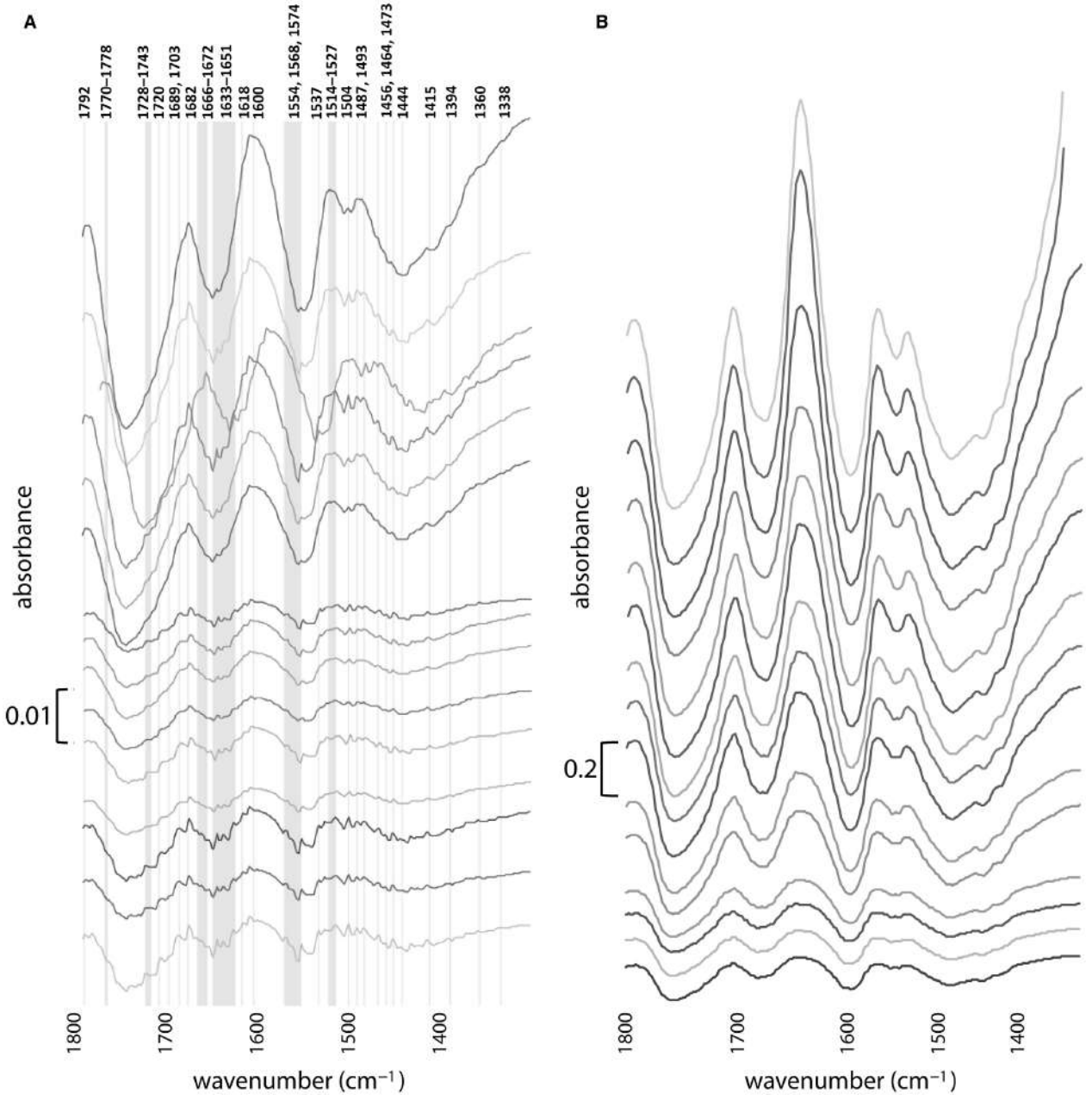

FIG. 5. Representative transmission Fourier transform infrared (FTIR) absorbance spectra in the range 1300–1800 cm^{-1}. A, Middle Marker horizon sample MM1. B, Hooggenoeg Formation H5c sample HC2. C, Footbridge Chert sample FC1. D, Josefsdal Chert sample JC1.

stretch), which forms a shoulder. Additionally, the aromatic C–H feature at 3010 cm^{-1} is visible in a limited number of spectra from both samples, although is close to being within the noise of the spectra.

In the aromatic/alkenic region, sample HC1 exhibits weak bands at 1340, 1348, 1356–1360 and 1433 cm^{-1} are attributed to CH_3 and a deviation at 1456 cm^{-1} assigned to asymmetrical CH_2 stretching. Bands at 1433 and 1456 cm^{-1} are attributed to C–H stretching from polysaccharides. Bands at 1392, 1415 and 1691 cm^{-1} are assigned to the symmetrical stretch of C–O, COO and the >C=O ester stretch, respectively, of carboxyl groups. The band at 1547 cm^{-1} is attributed to amide II, comprising C–N and N–H. Distinct bands at 1635–1649 cm^{-1} indicate highly conjugated C=O. Olefinic and aromatic groups, together with contributions from carboxyl COOH may account for the weak band at 1560 cm^{-1}. Carbonyl and carboxyl groups also account for well-defined bands at 1710 and 1720–1722 cm^{-1}, and weak features in some spectra at 1730 cm^{-1}, on the shoulder of the 1684 cm^{-1} Si–O peak. A band at 1481 cm^{-1} reflects an

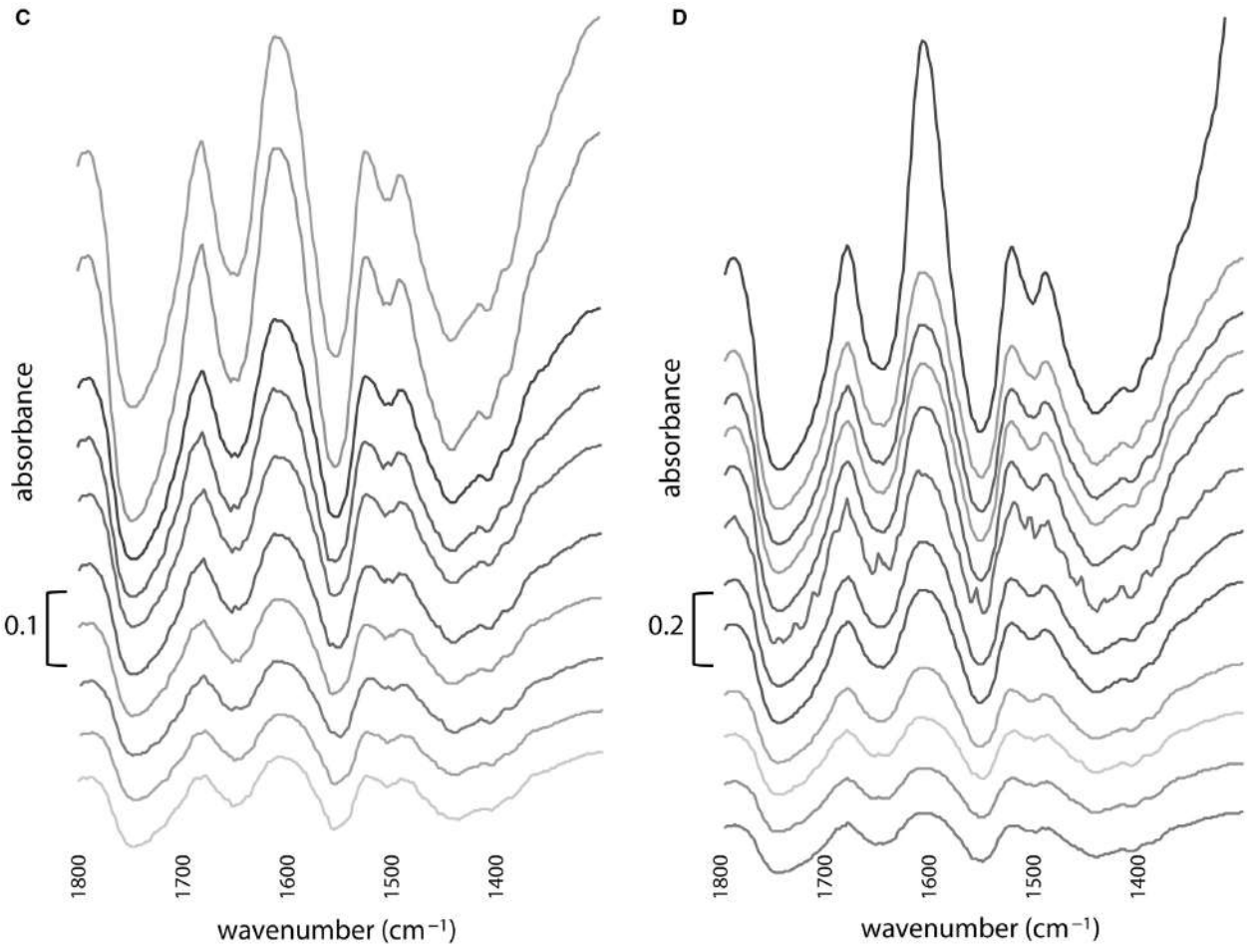

FIG. 5. (Continued)

aromatic ring stretch with a contribution from Si–O, and the bands at 1502 and 1604 cm^{-1} are attributed to aromatic ring stretching (C=C). A weak shoulder on the 1600 cm^{-1} C=C band at 1622 cm^{-1} may be δNH. Other peaks within the 1400–2000 cm^{-1} range at 1514–1527 and 1788–1792 cm^{-1} are interpreted as Si–O.

Sample HC2 (Fig. 5B) does not exhibit the CH_3 peak at 1348 cm^{-1}, but rather exhibits two peaks at 1543 and 1550 cm^{-1} attributed to C–H and N–H in amide II. HC2 exhibits additional features at 1489–1491 cm^{-1}, assigned to aromatic ring stretching, a wider array of bands reflecting highly conjugated C=O at 1628, 1643 and 1651 cm^{-1}, and two additional bands at 1714 and 1739 cm^{-1}, which are attributed to the >C=O ester stretch of carboxyl or carbonyl groups.

3.334 Ga Footbridge chert

Sample FC1 (03SA09 in the Orléans Lithothèque), comprising black-grey-white cherts with exceptionally well-preserved biofilm-like microbial horizons, exhibits weak, but consistently present, absorption bands in the aliphatic C–H stretching region at 2850, 2920–2925 and 2960 cm^{-1} (Fig. 4C) attributed to symmetrical and asymmetrical CH_2 and CH_3 stretching.

In the aromatic/alkenic region (Fig. 5C), sample FC1 exhibits weak bands at 1338, 1360 and weak features at 1435 cm^{-1} attributed to CH_3. Bands at 1435 and 1454 cm^{-1} are attributed to C–H stretching from polysaccharides. Bands at 1390–1394, 1415 and 1684–1689 cm^{-1} are assigned to the symmetrical stretch of C–O, COO and the >C=O ester stretch, respectively, of carboxyl groups. An additional band around 1739 cm^{-1} is also assigned to the >C=O ester stretch. Distinct bands at 1630–1649 cm^{-1} indicate highly conjugated C=O. Olefinic and aromatic groups may account for the weak band at 1554 cm^{-1}. Carbonyl and carboxyl groups are candidate identifications for weak bands at 1724–1732 cm^{-1}, on the shoulder of the 1684 cm^{-1} Si–O peak. A band at 1488–1491 cm^{-1} reflects an aromatic ring stretch with a contribution from Si–O. The bands at 1502 and

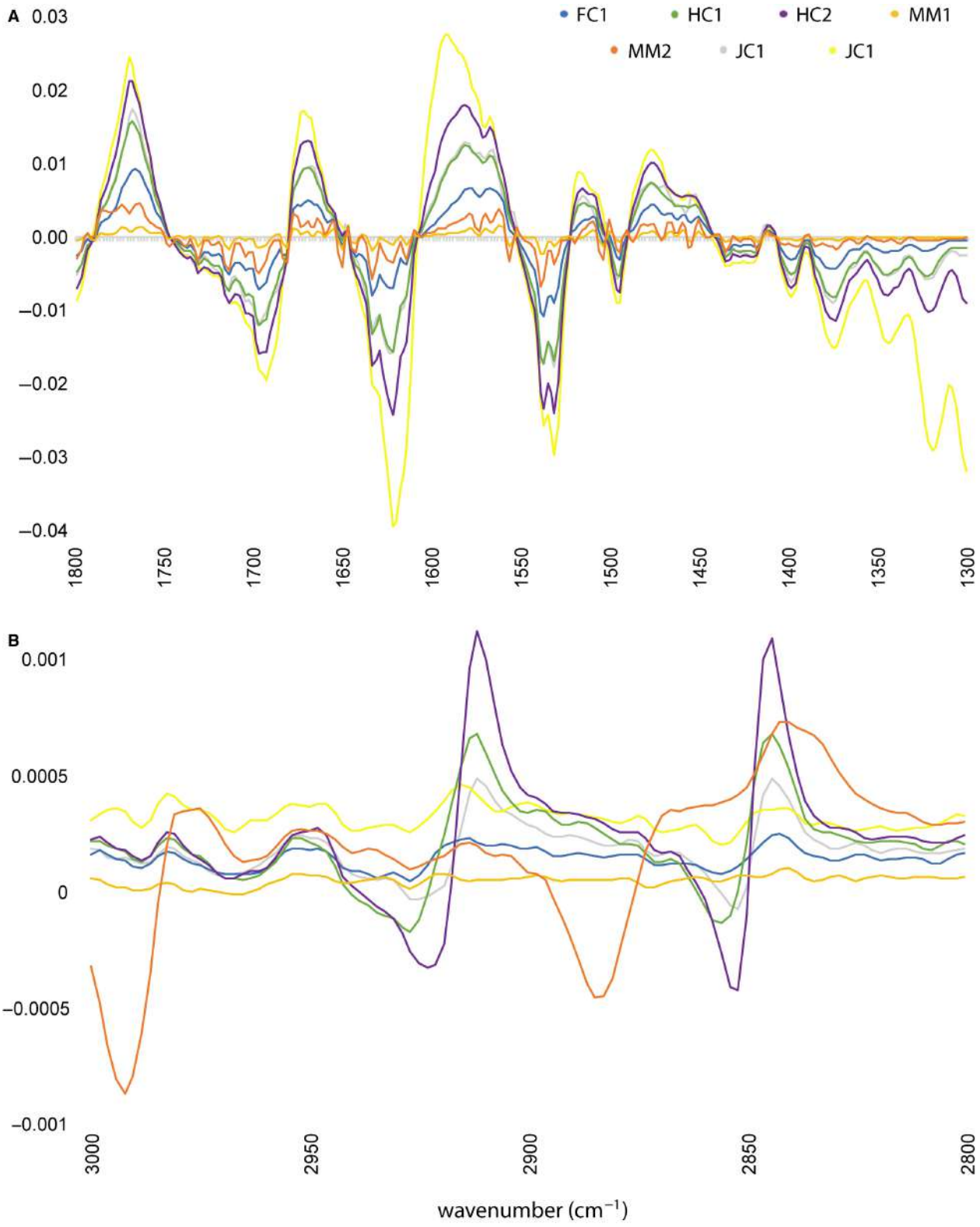

FIG. 6. Mathematical first-order derivative spectra averaged from each sample in the ranges: A, 1300–1800 cm^{-1}; B, 2800–3050 cm^{-1}. Spectral characteristics indicate similarity in biopolymer composition but differences in biopolymer concentrations, i.e. the absorbance ratio differs depending upon the sample. Deviations around 2850, 2880, 2925 and 2960 cm^{-1} indicate between-sample variation in aliphatic biochemistry.

1600 cm^{-1} are also attributed to aromatic ring stretching (C=C). Other peaks within the 1400–2000 cm^{-1} range at 1516–1523 and 1788 cm^{-1} are interpreted as Si–O.

3.33 Ga Josefsdal chert

FTIR spectra of sample JC1 (12SA18), a flat-laminated microbial mat with well-preserved individual laminae, show absorption bands of moieties in the aliphatic C–H stretching region (Fig. 4D) centred on 2850 (symmetrical CH_2 stretching), 2920 (asymmetrical methylene CH_2 stretching) and 2950–2960 cm^{-1} (asymmetrical CH_3 stretching), with a small number of spectra also showing a minor feature at 2870–2875 cm^{-1} corresponding to the symmetrical CH_3 stretch. A very minor band at 2890 cm^{-1} (C–H stretch) may exist as a shoulder to the broad feature centred on 2925 cm^{-1}. Two spectra from JC1 also exhibit the aromatic C–H bands at 3010 and 3030 cm^{-1}. JC2 (12SA36) shows only minor peaks at 2850 and 2925 cm^{-1} and weak deviations around 2960 cm^{-1}, suggesting a more minor aliphatic component.

In the aromatic/alkenic region (Fig. 5D), sample JC1 features bands at 1340, 1360 and 1433 cm^{-1} attributed to CH_3. Features at 1450, 1466 and 1470 cm^{-1} are also attributed to C–H stretching from polysaccharides. Bands at 1394 and 1714 cm^{-1} are assigned to the C–O and symmetrical >C=O ester stretch of carboxyl or carbonyl groups. The strong band at 1415 cm^{-1} is attributed to COO from carboxylate, while bands at 1572, 1682 and 1705 cm^{-1} reflect C=O and COOH from carboxyl, augmented by an Si–O band. Bands at 1730–1734 and 1747 cm^{-1} (on the shoulder of the 1684 cm^{-1} Si–O peak) are further evidence for a strong carbonyl–carboxyl contribution to JC1. The band at 1540 cm^{-1} is attributed to amide II, comprising C–N and N–H. Bands at 1635–1653 cm^{-1} denote highly conjugated C=O bonds. Furthermore, a small feature at 1670 cm^{-1} is attributed to alkyl or phenyl groups. Olefinic and aromatic groups, together with contributions from carboxyl COOH may account for the weak band at 1554–1558 cm^{-1}. A band at 1490 cm^{-1} reflects an aromatic ring stretch with a contribution from Si–O, and the bands at 1502 and 1600 cm^{-1} provide evidence of aromatic ring stretching (C=C). Other peaks within the 1400–2000 cm^{-1} range at 1518–1522 and 1788 cm^{-1} are interpreted as Si–O.

In general, the intensity and diversity of peaks, particularly within the aliphatic stretching region, are considerably higher in JC1 than JC2, indicating superior preservation of structural variation in the former. A smaller complement of bands in the aromatic/alkenic region of JC2 also supports this. JC2 exhibits only a single weak feature at 1454 cm^{-1} attributable to C–H stretching in polysaccharides and limited weak features at 1684–1687 and 1734 cm^{-1}, suggesting lower concentrations of preserved carboxyl and carbonyl groups. The 1710 cm^{-1} feature attributed to the >C=O ester stretch of carboxyl or carbonyl groups is very minor and the features at 1540, 1554–1558 and 1572 cm^{-1} are absent.

DISCUSSION

FTIR spectra may be evaluated both qualitatively, to identify preserved molecular complexity, and quantitatively, since the intensity of an absorption band increases proportionally with its frequency in the corresponding molecule or functional group (Marshall *et al.* 2005; Chen *et al.* 2015). FTIR spectra from the studied mats show similar overall spectral characteristics (Fig. 3), but fine-scale differences, particularly the variable concentrations and compositions of aliphatic moieties (CH_2 and CH_3; Figs 4, 5). Averaging the mathematical first-order derivative spectra of each horizon reveals strong similarities amongst the samples, indicating that the same or similar range of chemical components are present in all carbonaceous materials (Table 1). The major source of variability occurs in the aromatic and especially aliphatic regions (Fig. 6), best explained as differential peak intensity reduction due to the metamorphic maturation of carbonaceous materials (Fraser *et al.* 2014; Jardine *et al.* 2015). The many spectral features identified indicate that relics of diverse molecules and functional groups are present in this carbonaceous material.

The following discussion initially addresses the origin of the FTIR signals and evaluates whether diagenetic overprinting can account for the spectral variation observed. Secondly, we describe the (bio)polymer compositions preserved, and use the aliphatic chain length and branching model of Lin & Ritz (1993) to determine the lengths and degree of branching of aliphatic moieties. Using this information, we follow the approach of Igisu *et al.* (2009, 2018), complemented by a detailed set of statistical tests, to distinguish the contributions of the domains Bacteria and Archaea to these microbial mats and demonstrate measurable differences between individual mat-bearing horizons. We conclude with a brief discussion of the implications of this exceptional biopolymer preservation for microbial silicification rates.

Origin of FTIR signals: biology vs diagenesis

FTIR spectra, although preserving a unique biochemical record, are not immune to the effects of organic material maturation through diagenesis; even the FTIR spectra of recalcitrant molecules begin to alter at around 250–300°C (Fraser *et al.* 2014). Since the samples studied herein have

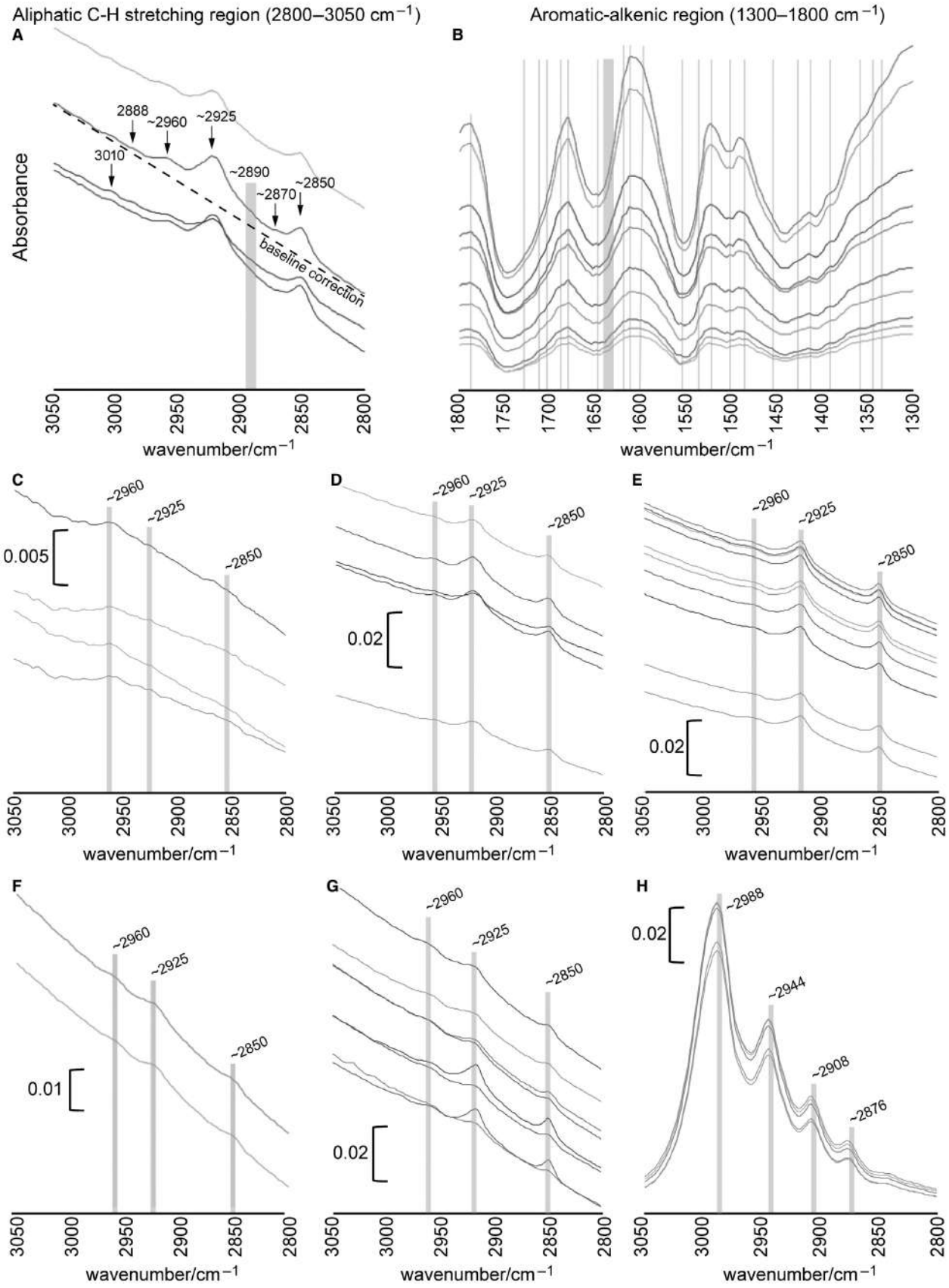
Aliphatic C-H stretching region (2800–3050 cm−1)
Aromatic-alkenic region (1300–1800 cm−1)
A
B
Absorbance
2888
~2960
~2925
3010
~2890
~2870
~2850
baseline correction
3050 3000 2950 2900 2850 2800
wavenumber/cm−1
1800 1750 1700 1650 1600 1550 1500 1450 1400 1350 1300
wavenumber/cm−1
C
0.005
~2960
~2925
~2850
wavenumber/cm−1
D
0.02
~2960
~2925
~2850
wavenumber/cm−1
E
0.02
~2960
~2925
~2850
wavenumber/cm−1
F
0.01
~2960
~2925
~2850
wavenumber/cm−1
G
0.02
~2960
~2925
~2850
wavenumber/cm−1
H
0.02
~2988
~2944
~2908
~2876
wavenumber/cm−1

undergone metamorphic temperatures of 285–400°C (Xie *et al.* 1997; Tice *et al.* 2004; Hickman-Lewis *et al.* 2020*b*) it is necessary to evaluate whether original biochemistry or post-depositional maturation dominates the FTIR signal.

Igisu *et al.* (2009) and Fraser *et al.* (2014) conducted experimental maturation of carbonaceous materials and noted three trends in spectral evolution: (1) aliphatic/aromatic ratios reduced due to decreased peak intensities particularly within the aliphatic region (consistent with low absorption intensities in Fig. 4); (2) spectral detail becomes increasingly simplified with increasing maturity due to the loss of various water-soluble groups (consistent with overall spectral form in Fig. 3); and (3) relative changes in spectral characteristics (e.g. relative concentrations of aliphatic vs aromatic molecules) change predictably with increasing maturation. Jardine *et al.* (2015) also found that chemical alteration under heat led towards a general homogenization (simplification) of spectral characteristics, and concomitant weakening of the taxonomically indicative aliphatic peaks. Critically, however, it remains possible to recover taxonomic signals even after extensive alteration and time (e.g. Palaeozoic sporopollenin; Steemans *et al.* 2010; Fraser *et al.* 2012) and chemically distinguish taxa even after alteration (Jardine *et al.* 2015). Although some studies have suggested that aliphatic molecules may be produced during diagenesis (e.g. Kodner *et al.* 2009), this is not sustained by either experimental work or observation (Gupta *et al.* 2007; Igisu *et al.* 2009; Fraser *et al.* 2014), and is thus more logically explained as the selective preservation of non-hydrolysable aliphatic macromolecules derived from the original biomass (de Leeuw *et al.* 2006). Oxidative polymerization of non-fossilized organic materials, advocated as a method of diagenetic aliphatic increase by Versteegh & Blokker (2004), could not have occurred in the studied silicified sediments since microquartz (chert) is impermeable; there is therefore no possibility for secondary organic moieties to form on or within this already fossilized biomass. As highlighted in the Introduction, membrane lipid compositions generally dominate the taxonomically indicative aliphatic window of FTIR spectra even after fossilization (Marshall *et al.* 2005; Igisu *et al.* 2006, 2009, 2018).

Overall, alterations in FTIR spectra primarily occur within the oil window or zeolite-grade conditions of metamorphism (Igisu *et al.* 2009; Fraser *et al.* 2014; Hackley *et al.* 2017) after which longer-term maturation produces only minor changes (Igisu *et al.* 2009; Jardine *et al.* 2015). Selective preservation of lipids relative to other cellular components may occur during post-mortem diagenesis, but the relative preservation of the aliphatic CH_2 and CH_3 bands that enable membrane lipid identification is similar (Igisu *et al.* 2009). Therefore, despite the muting of spectral characteristics during diagenesis, variation in spectra from silicified microbial mats is overwhelmingly explained by diversity in original biomass composition. The fact that aliphatic, aromatic and other carbon-bearing groups are identified (Figs 4, 5) in this unambiguously microbial material evidences partial degradation and kerogenization consistent with the thermal history of the host rock (Bonneville *et al.* 2020). All of the above evidence is singularly supportive of our FTIR spectra being dominated by biology, not diagenesis, and justifies the use of these spectra for taxonomic distinction. This is consistent with recent findings using advanced geochemistry demonstrating that diagenesis does not obliterate all biochemical specificity in even the most ancient fossils (Marshall *et al.* 2005; Igisu *et al.* 2006, 2009, 2012, 2018; Westall *et al.* 2011, 2015; Alleon *et al.* 2016*a*; Hickman-Lewis *et al.* 2017, 2018*a*, 2020*b*; Wacey *et al.* 2017).

Statistically significant differences in biopolymer composition between microbial mats

In order to evaluate variation in biopolymer compositions between and within samples and between horizons, we conducted a number of statistical analyses to demonstrate the variation of spectral parameters (Figs 8–10; Table 2). Even simple statistical treatments (box plots and scatter graphs) evince a clear variation in aliphatic molecules and functional groups in spite of the highly aromatized

FIG. 7. Details and interpretation of IR spectra from the studied samples. A, summarized band identification in the aliphatic stretching region (2800–3050 cm^{-1}), with aliphatic CH_2 (methylene) and CH_3 (end-methyl) bonds identified. B, summarized band identification in the aromatic/alkenic region (1300–1800 cm^{-1}); lines indicate band identification; see main text and Figure 5A for details. C–G, examples of the aliphatic stretching region for mats from: C, the Middle Marker horizon (sample MM1); D–E, the Hooggenoeg Formation H5c (samples HC1 and HC2, respectively); F, the Footbridge Chert (sample FC1); G, the Josefsdal Chert (sample JC1). H, FTIR characterization of the carbon-based cyanoacrylate adhesive used within the same region (2800–3050 cm^{-1}) demonstrating that all bands identified in Figure 3 and parts A–G of this figure are not contaminated by adhesive, which is characterized by high-intensity absorption bands at 2988, 2944, 2908, and 2876 cm^{-1} within the aliphatic C–H stretching region (shown) and weaker bands at 1450 and 1375 cm^{-1} in the aromatic-alkenic region (not shown). All horizontal axes represent wavenumber and vertical axes represent absorbance.

TABLE 1. Band and peak identifications in FTIR spectra.

Wavenumber (cm^{-1})	Designation	Occurrence (sample number)
1338, 1340, 1348, 1356–1360	CH_3	MM1, MM2, HC1, HC2, FC1, JC1
1433–1435, 1454–1456, 1470	CH_2, C–H stretch from polysacharides	MM1, MM2, HC1, HC2, FC1, JC1
1444, 1464	C–H stretching with aromatic ring stretching	MM1, MM2, HC1, HC2, FC1
1489–1491	Aromatic ring stretching	HC2
1373	CH_3	MM2
1390–1394	C–O	MM1, MM2, HC1, HC2, FC1, JC1
1415	COO	MM1, MM2, HC1, HC2, FC1, JC1
1430, 1433	Aliphatic C–H stretching	MM2, HC2
1469–1473	Ester C=O	MM1, MM2
1481, 1487–1493	Aromatic ring stretches with a contribution from Si–O	MM1, MM2, FC1, JC1
1502–1504	C=C	All
1514–1527	Si–O	All
1537	Aliphatic COOH	MM1(?), MM2(?)
1540–1543, 1547, 1550	Amide II (C–N and N–H)	HC1, HC2, JC1
1554–1560, 1568, 1572–1574	Olefinic and aromatic groups, with carboxyl COOH	MM1, MM2, HC1(?), HC2(?), FC1(?), JC1, JC2
1600–1604	C=C	All
1618–1622	δNH	MM1(?), MM2(?), HC1(?), HC2(?)
1628–1653	Highly conjugated C=O	MM1, MM2, HC1, HC2, FC1
1666, 1672	Si–O	All
1670	Alkyl and/or phenyl groups	MM1(?), MM2(?), JC1
1682	Si–O	All
1684–1689, 1691, 1703–1705	Carbonyl C=O and carboxyl COOH	MM1, MM2, HC1, HC2, JC1, JC2
1710, 1714, 1720–1722	Carbonyl and carboxyl groups; >C=O ester stretch	MM1, MM2, HC1, HC2, FC1, JC1, JC2(?)
1728–1747	>C=O ester stretch	MM1, MM2, HC1(?), HC2, FC1, JC1, JC2
1770–1778	Ester C=O	MM1, MM2
1788–1792	Si–O	All
2850	Symmetrical CH_2 stretch	All
2870–2875	CH_3	MM2, HC2(?)
2890	C–H stretch	HC1(?), JC1(?)
2920–2925	Asymmetrical methylene CH_2 stretch	All
2960	Asymmetrical end-methyl CH_3 stretch	MM1, MM2, HC1, HC2, FC1, JC1, JC2(?)
3010, 3030	Aromatic C–H	JC1

Identifications were made after Socrates (1980), Painter *et al.* (1985), Benning *et al.* (2004), Marshall *et al.* (2005), Igisu *et al.* (2009), Guido *et al.* (2013) and Chen *et al.* (2015).

structure of the carbonaceous materials. This is evident from the large ranges in CH_3/CH_2, CH_2/CH_3, Abs_{1710}/Abs_{1600} and Abs_{2925}/Abs_{1710} ratios, whereas the aliphatic/aromatic ratio remains uniformly low in all samples (Fig. 8). Comparison of the $R_{3/2}$ ratio with measured values from extant biology (bacterial and archaeal cell components), microfossils from Proterozoic horizons and organic materials from the contemporaneous Dresser Formation (Fig. 8A; Igisu *et al.* 2009, 2012, 2018, 2019; Qu *et al.* 2015; Bonneville *et al.* 2020) indicates that most of the microbial mats studied exhibit a wide range in this ratio and significant overlaps both with extant and extinct biology, probably reflecting a community signal. The precise meaning of this signature for microbial diversity in the Palaeoarchaean is addressed below. Whereas the Josefsdal and Footbridge cherts (samples JC1, JC2 and FC1) show considerable overlap in $R_{3/2}$ and CH_2/CH_3 values (Fig. 8A, B; considering the range between the 25th and 75th percentiles), the ratios in the Middle Marker and Hooggenoeg Chert mats (especially HC2) show significantly different values. Taken together, CH_3/CH_2 and CH_2/CH_3 ratios suggest that the Hooggenoeg and Middle Marker mats were dominated by Bacteria (characterized by long, unbranched membrane lipids) and

Archaea (characterized by shorter, highly branched membrane lipids), respectively, whereas the other mats were inhabited by mixed consortia. Concentrations of aliphatic moieties are relatively similar throughout all samples and lower than in reported datasets for Proterozoic material; all aliphatic/aromatic ratios measured were below 0.07 (Fig. 8C). Abs_{1710}/Abs_{1600} ratios vary widely between and within samples (Fig. 8D), whereas Abs_{2925}/Abs_{1710} ratios vary widely between, but to a lesser extent within, samples (Fig. 8E). In summary, box plots indicate diverse aliphatic and carbonyl/carboxylic compositions in the studied carbonaceous materials. Aliphatic ratios resemble the biopolymer compositions detected in contemporaneous (Igisu *et al.* 2018) and younger (Marshall *et al.* 2005; Igisu *et al.* 2006, 2009; Javaux & Marshall 2006; Qu *et al.* 2015) biogenic organic materials.

Analysis of variance (ANOVA) found significant differences in CH_2/CH_3 and CH_3/CH_2 with high coefficients of determination (0.767 and 0.820, respectively) and $p < 0.01$ (Table 2). Samples were grouped using Tukey's and REGWQ (Ryan–Einot–Gabriel–Welsh Studentized Range Q) tests; in all but two cases (the CH_3/CH_2 ratios of HC2 and JC2) these groupings were identical for the two tests (Table 2). A confidence interval of $p < 0.05$ was not attained in comparisons of the aliphatic/aromatic, Abs_{1710}/Abs_{1600} and Abs_{2925}/Abs_{1710} ratios, indicating that the means of these ratios are not statistically distinct across the seven studied samples; this concurs with the lack of sample-specific grouping in box plots (Fig. 8D, E).

Two-sample Student's *t*-tests were conducted on all spectral parameters from all pairs of samples. These tests, determining whether mean values between samples are significantly different, invariably support the distinction of samples by the other tests. Three illustrative examples follow. Comparing samples HC2 and MM2, which are the most distinct based on box plots and PCA (see below), and joint most distinct based on ANOVA, the Student's *t*-test finds that the null hypothesis can be rejected at a confidence level of $p < 0.01$ for CH_2/CH_3, CH_3/CH_2, Abs_{1710}/Abs_{1600} and Abs_{2925}/Abs_{1710} ratios, but cannot be rejected for the aliphatic/aromatic ratio; i.e. the two samples are significantly distinct in four out of five tested spectral parameters. Comparing MM1 and MM2, which directly overlap in all other tests (box plots, ANOVA, PCA), no spectral parameters, except for the Abs_{2925}/Abs_{1710} ratio, enable rejection of the null hypothesis; i.e. the two samples are similar in four out of five parameters. Comparing HC1 and JC1, which partly overlap in box plots, scatter plots, ANOVA and PCA, the Student's *t*-test finds significant differences in the CH_3/CH_2 and Abs_{2925}/Abs_{1710} ratios but is unable to reject the null hypothesis for the CH_2/CH_3, aliphatic/aromatic and Abs_{1710}/Abs_{1600} ratios; i.e. the samples are similar in three out of five parameters.

Scatter plots further sustain these distinctions: the CH_3/CH_2 ratio (and by extension its reciprocal CH_2/CH_3) shows sample-specific grouping independent of aliphatic/aromatic ratios (Fig. 9A), whereas overlapping groupings of ratios incorporating aliphatic and carbonyl/carboxylic groups (Fig. 9B–F) suggests that most between-sample and within-sample variation (even in the same chert) results from the relative concentrations of aliphatic and, to a lesser extent, carbonyl/carboxylic groups. Since, in fossilized microbial mats, carbonyl/carboxylic groups are more likely to be derived from extracellular polymeric substances whereas aliphatic compounds derive from cell membranes, we add statistical support to the findings of Igisu *et al.* (2009) that variations in the taxonomic indices of FTIR spectra (and by extension, carbonaceous materials) are dominated by membrane lipids.

Finally, all spectral data were subjected to principal component analysis (PCA), an ordination technique based on an orthogonal transformation to convert a set of observations into a minimal number of possibly correlated dimensions (the eponymous principal components). Considering the CH_3/CH_2, Abs_{1710}/Abs_{1600} and Abs_{2925}/Abs_{1710} ratios as the key spectral data from which taxonomic conclusions can be made, the first two PCA axes account for 89.65% of total variance in the dataset (Fig. 10A). Since the aliphatic/aromatic ratio is relatively constant (Fig. 8C), this indicates very clear differences between the aliphatic fractions of each sample. PCA axis 1, accounting for 68.03% of the variance, clearly separates samples with high (MM1, MM2) and low (HC2, JC1 and JC2) CH_3/CH_2 ratios, whereas some overlap exists between samples FC1, JC1, JC2 (to a lesser extent) and HC1. FC1, exhibiting the widest 25th–75th percentile range in CH_3/CH_2, predictably overlaps with both groups. A second PCA analysis, as above but excluding the CH_3/CH_2 ratio, explained only 78.89% of variance (Fig. 10B), confirming that most variance is captured within the aliphatic fractions and that higher intra-sample variability occurs in the carbonyl/carboxylic groups (Figs 8D–E, 9D–F). This is expected since these biomass components are localized within specific portions of microbial mats and would thus be heterogeneously distributed in the aliphatic residues. Since an overwhelming percentage of total variance (almost 90%) can be explained through the PCA analyses that reflect the CH_3/CH_2 ratios, we advocate these as the crucial parameters for explaining sample differences related to composition and taxonomy.

In conclusion, a suite of statistical techniques shows similarities and differences between the spectral characteristics of the studied samples. Particularly strong distinctions emerge in the CH_2/CH_3 and CH_3/CH_2 ratios which, as outlined above, are derived directly from the Palaeoarchaean organisms that constructed these microbial mats and thus have taxonomic significance for their

classification (see Lin & Ritz 1993; Marshall *et al.* 2005; Igisu *et al.* 2009, 2012).

Biopolymer composition, aliphatic chain length and branching

Peak identifications of the following molecules and functional groups were made: (1) CH_3, CH_2 and other C–H stretching attributed to polysaccharides; (2) C–O, COO and the >C=O ester stretch of carboxyl groups; (3) aliphatic carboxyl COOH; (4) ester C=O and highly conjugated carbonyl C=O; (5) olefinic and aromatic groups; (6) diverse carbonyl and carboxyl groups; (7) alkyl and/or phenyl groups; (8) aromatic ring stretches (C=C); and (9) δNH. Other peaks were interpreted as Si–O. Although absorption intensity varies between samples, the consistency of wavenumbers attributable to specific moieties and the large number of band identifications that support other band identifications, for example numerous carbonyl–carboxyl and aliphatic groups, confirm the preservation of biomolecular diversity. No other reasonable explanation exists for the recurrent observation of spectral diversity in microbial structures. This demonstrates that, despite their great age and more than 3 Ga of geological processing, even the most ancient microbial mats preserve a rich complement of biomolecules testament to a wealth of biological diversity in their architect communities.

The carbonaceous materials constituting these mats therefore comprise predominantly polyaromatic hydrocarbon frameworks with small amounts of aliphatic C–H groups, among others. All horizons show features in the aliphatic stretching region between 2800 and 3050 cm^{-1}, namely bands at 2850 cm^{-1} (symmetrical CH_2 stretching), 2920–2925 cm^{-1} (asymmetrical methylene CH_2 stretching) and 2950–2960 cm^{-1} (asymmetrical CH_3 stretching), with many spectra also showing a minor feature at 2870–2875 cm^{-1} corresponding to the symmetrical CH_3 stretch (Fig. 7A). Other minor peaks, e.g. 2988 cm^{-1}, which are represented in only a small number of spectra (e.g. MM1, Fig. 7C), are more challenging to identify. The peak at 2988 cm^{-1} is also exhibited by the spectra of the carbon-based cyanoacrylate adhesive used in thin section preparation (Fig. 7H), and could be contamination. We do not believe, however, that this is the case, primarily because the significant differences in absorption intensity (an order of magnitude) between the spectra of the adhesive and those of the carbonaceous materials suggest that the 2988 cm^{-1} has different origins in each instance. Secondly, spectra exhibiting the 2988 cm^{-1} band exhibit a second band at 3010 cm^{-1}, which is also attributable to the C–H aromatic stretch. Thirdly, no other bands characterizing the spectrum of the adhesive (2944, 2908, and 2876 cm^{-1}) exist in these spectra. We consider that to find only one adhesive band at such low intensity is inconsistent with contamination and interpret the 2988 cm^{-1} band as indigenous to biogenic carbonaceous matter.

The CH_2/CH_3 ratio described by Lin & Ritz (1993) provides an estimate of the chain length of the aliphatic hydrocarbon moiety bridging the aromatic structure, together with its degree of branching. Naturally matured kerogens, when compared with artificially matured kerogens, indicate that the CH_2/CH_3 ratio undergoes only a minor initial decrease during maturation (Lin & Ritz 1993; Lis *et al.* 2005), suggesting that aliphatic chains become only slightly shorter and/or more branched during low-grade metamorphism. This is due to the slight preferential degradation of methylene CH_2 over end-methyl CH_3 under similar thermal alteration conditions (Igisu *et al.* 2009). The CH_2/CH_3 ratios observed in the studied mats fall within the range of other micropalaeontological samples (Arouri *et al.* 1999; Marshall *et al.* 2005; Igisu *et al.* 2009) and, as with $R_{3/2}$ ratios, show statistically significant variation between samples (Fig. 8B). Using the simplified *n*-alkane model of Lin & Ritz (1993), we calculate that the Middle Marker mats are characterized by aliphatic biopolymers with short, highly branched *n*-alkanes with chain lengths of between 5 and 6; the Hooggenoeg Chert H5c mats are characterized by longer, less branched chains of 7–13 units; and the Footbridge and Josefsdal cherts by broadly similar intermediate values of 5–9 and 6–9, respectively (Fig. 8B; Table 3). An outlier point in Josefsdal Chert sample JC1 (Fig. 8B) may represent a region of increased concentration of long (chain length 11–12), unbranched aliphatic biopolymers.

Microbial diversity within Palaeoarchaean mats

Understanding microbial diversity in mat-building communities from the Archaean is a critical outstanding question in Precambrian palaeobiology. The aliphatic fraction (between 2850 and 2960 cm^{-1}) is a taxonomically indicative signal, and our statistical analyses above have demonstrated that this fraction exhibits clear differences between the studied samples and horizons (Figs 4, 6B, 7). The aliphatic composition of membrane proteins varies between the three domains of life: Bacteria, Archaea and Eukarya (Atlas 1989; Igisu *et al.* 2012; Albers & Meyer 2011). This differential signal can be applied to the fossil record, evidenced, for example, by FTIR signals of cyanobacterial microfossils that are consistent with bacterial affinities (Igisu *et al.* 2006, 2009, 2018) but inconsistent with archaeal or eukaryotic affinities (Marshall *et al.* 2005; Bonneville *et al.* 2020). FTIR analyses of Palaeoarchaean

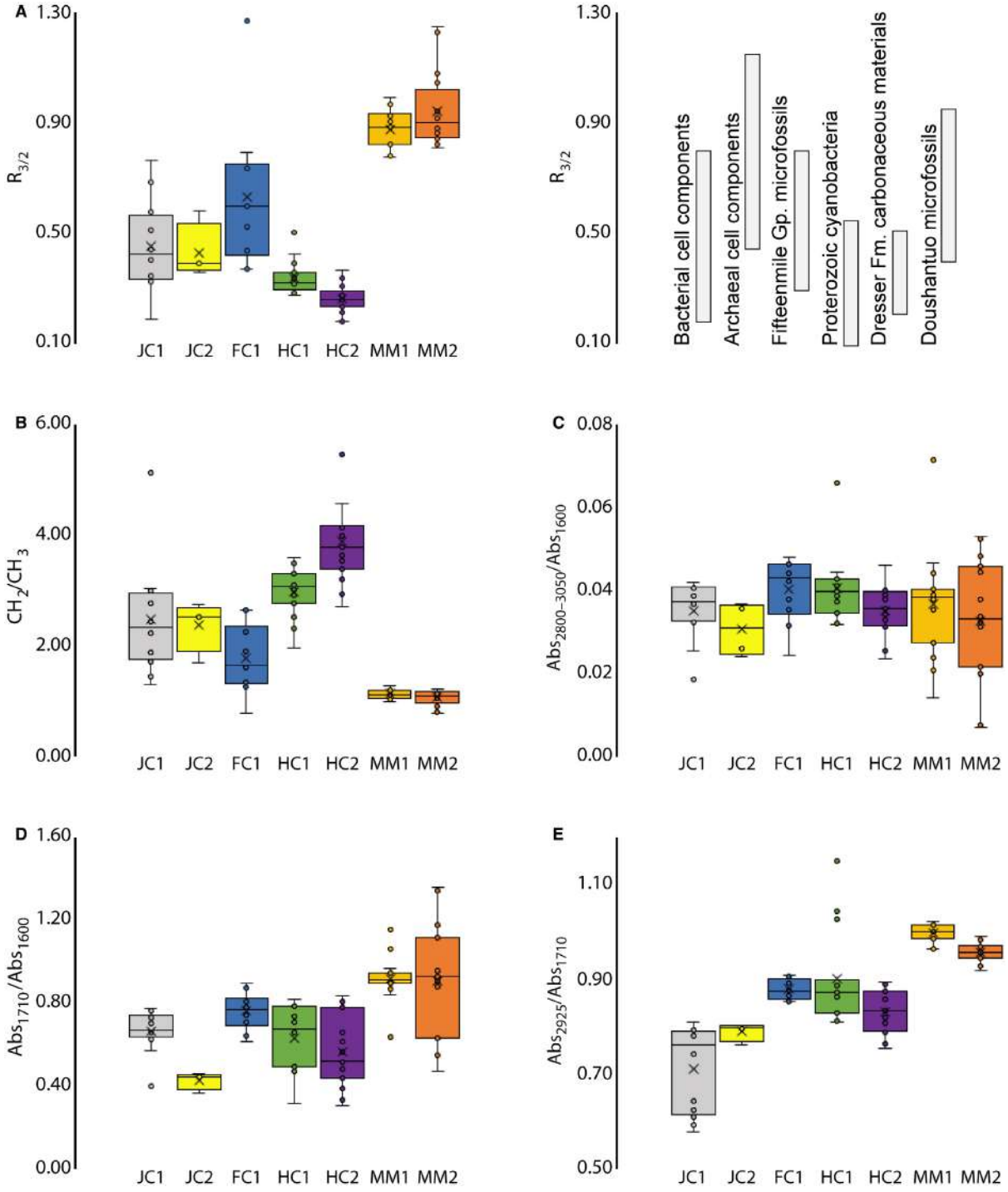

FIG. 8. Box plots showing distributions of spectral characteristics. A, CH_3/CH_2 ($R_{3/2}$) with measured values from extant biology (bacterial and archaeal cell components), microfossils from Proterozoic horizons and organic materials from the contemporaneous Dresser Formation (compiled after Igisu *et al.* 2009, 2012, 2018, 2019; Qu *et al.* 2015; Bonneville *et al.* 2020). B, aliphatic ratio CH_2/CH_3 shows considerable overlap for Josefsdal (JC) and Footbridge (FC) samples and significantly different values in the Middle Marker (MM) and Hooggenoeg chert (HC) mats (especially sample HC2). C, the aliphatic/aromatic ratio ($Abs_{2800–3050}/Abs_{1600}$) is similar throughout all samples. D, Abs_{1710}/Abs_{1600} ratios vary widely between and within samples. E, Abs_{2925}/Abs_{1710} ratios vary widely between, but to a lesser extent within, samples. In all box plots, the cross indicates the mean value, the horizontal line indicates the median value, and circles outside the box denote outliers. [Correction added on 13 October 2020 after first publication: the y-axis labels in part C have been corrected in this version.]

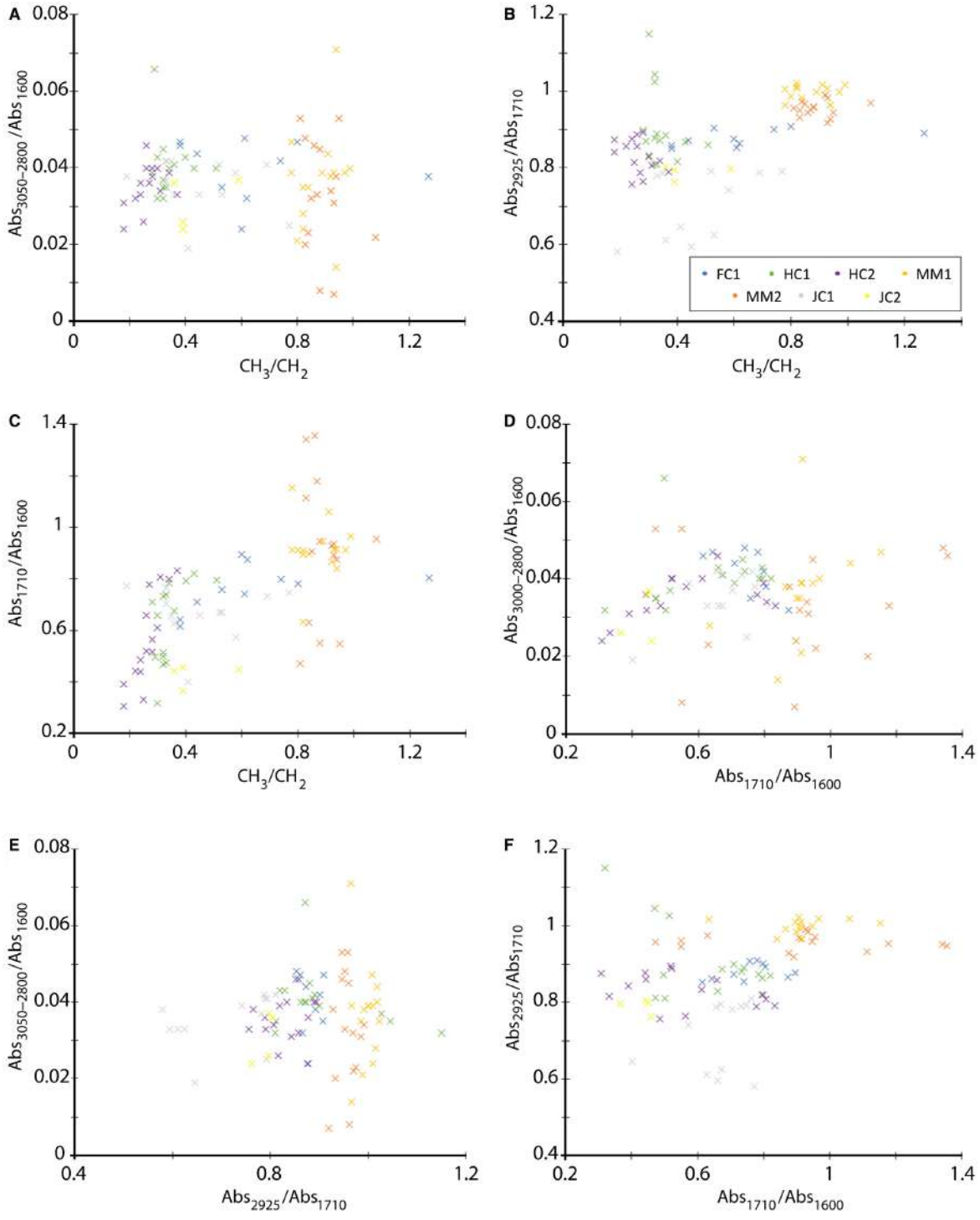

FIG. 9. Bi-dimensional scatter plots showing variation in spectral characteristics between samples. A, $R_{3/2}$ ratio vs aliphatic/aromatic ($Abs_{3050-2800}/Abs_{1600}$) ratio showing that while the former is highly variable between samples, the latter is essentially constant. B, $R_{3/2}$ ratio vs aliphatic/carbonyl–carboxyl (Abs_{2925}/Abs_{1710}) ratio, indicating a weak positive correlation. C, $R_{3/2}$ ratio vs carbonyl–carboxyl/aromatic (Abs_{1710}/Abs_{1600}) ratio, indicating a weak positive correlation. D, carbonyl–carboxyl/aromatic (Abs_{1710}/Abs_{1600}) ratio vs aliphatic/carbonyl–carboxyl (Abs_{2925}/Abs_{1710}) ratio, showing no meaningful correlation. E, aliphatic/carbonyl–carboxyl (Abs_{2925}/Abs_{1710}) ratio vs aliphatic/aromatic ($Abs_{3050-2800}/Abs_{1600}$) ratio, showing no meaningful correlation. F, carbonyl–carboxyl/aromatic (Abs_{1710}/Abs_{1600}) ratio vs aliphatic/carbonyl–carboxyl (Abs_{2925}/Abs_{1710}) ratio, showing no meaningful correlation. Taking all scatter plots into consideration, we find that only the $R_{3/2}$ ratio exhibits significant and meaningful variation between samples.

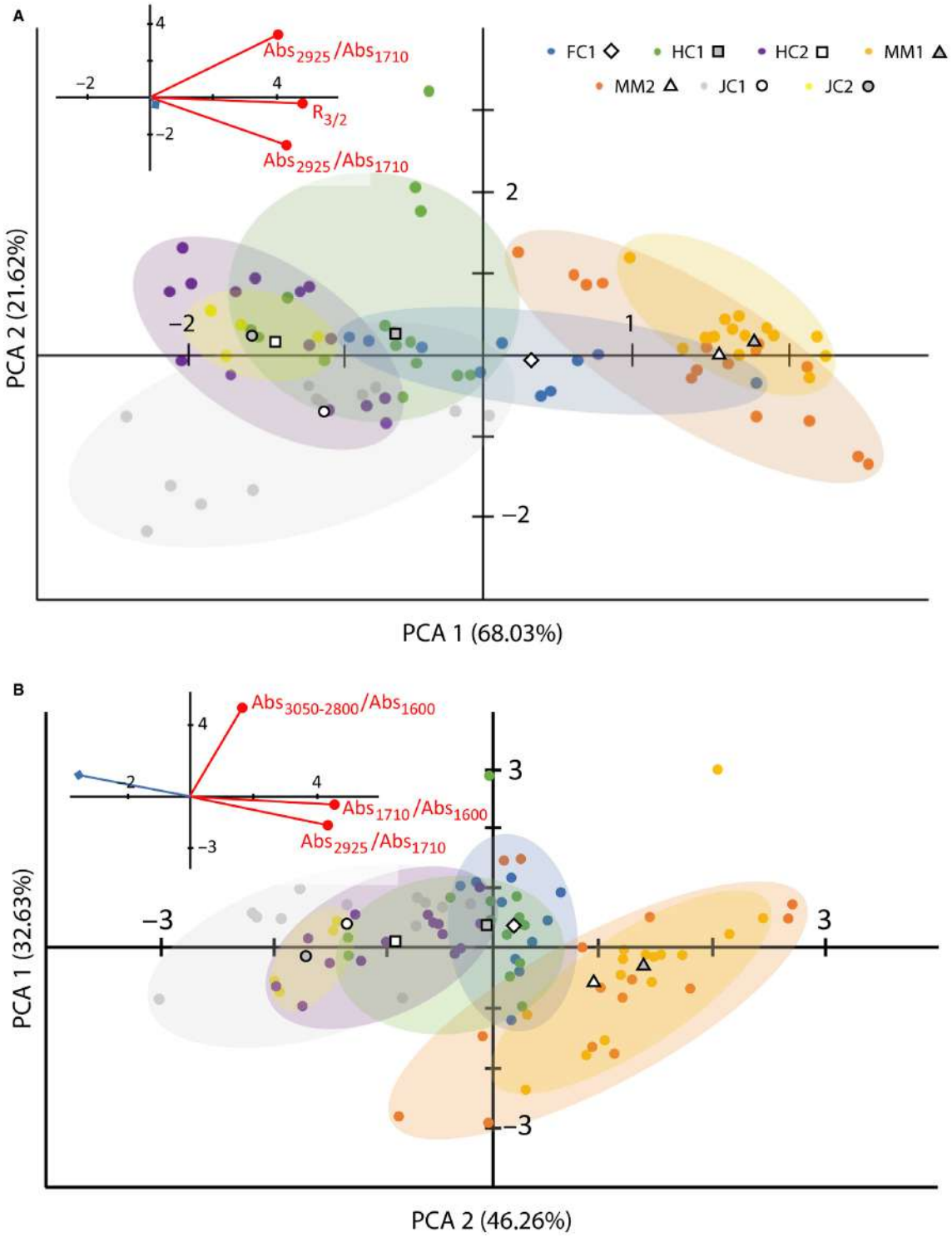

FIG. 10. Principal components analysis (PCA) of spectral parameters, considering: A, the CH_3/CH_2, Abs_{1710}/Abs_{1600} and Abs_{2925}/Abs_{1710} ratios, explaining 89.65% of variance in the dataset; PCA axes 1 and 2 were sufficient to explain most variance in the data; percentages in parentheses indicate the variance explained by that axis; B, the $Abs_{3050–2800}/Abs_{1600}$ (aliphatic/aromatic), Abs_{1710}/Abs_{1600} and Abs_{2925}/Abs_{1710} ratios, explaining only 78.89% of variance in the data. Insets show loadings plots; blue diamonds denote the factors ($Abs_{3050–2800}$ in A and $R_{3/2}$ in B). Coloured regions were drawn to conservatively include all data from a single sample, discounting outliers. This indicates both similarities (overlap) and differences between the spectral characteristics of the samples approximately following the PCA axes. Coloured points indicate individual analyses and grey/white symbols (triangles, squares, diamonds, circles) indicate the centroid of each point cloud.

TABLE 2. ANOVA results.

Unit	Sample	Grouping based on Tukey's test	Grouping based on REGWQ test	Coefficient of determination	*p*-value
CH_2/CH_3					
Middle Marker horizon	MM1	D	D	0.767	5.12×10^{-23}
	MM2	D	D		
Hooggenoeg Chert H5c	HC1	B	B		
	HC2	A	A		
Footbridge Chert	FC1	C–D	C–D		
Josefsdal Chert	JC1	B	B		
	JC2	B–C	B–C		
CH_3/CH_2 ($R_{3/2}$ value)					
Middle Marker horizon	MM1	A	A	0.820	2.13×10^{-27}
	MM2	A	A		
Hooggenoeg Chert H5c	HC1	C–D	C–D		
	HC2	C	D		
Footbridge Chert	FC1	B	B		
Josefsdal Chert	JC1	C	C		
	JC2	C	C–D		

Groupings of samples are based on Tukey's and Ryan–Einot–Gabriel–Welsh Studentized Range Q (REGWQ) tests. The coefficient of determination is high in each case, and all sample differences are deemed statistically significant with a *p*-value much lower than 0.01.

mats presented herein thus provide a means of linking taxonomy and phylogeny to mat fabrics through *in situ* chemistry. Since FTIR spectral features diagnostic of precursor biology are resilient to diagenetic degradation (Lin & Ritz 1993; Peters *et al.* 2005; Lis *et al.* 2005; Steemans *et al.* 2010; Fraser *et al.* 2014), the aliphatic moieties preserved reflect compositional variation in precursor (architect) biological materials at the moment of fossilization of the microbial mat.

Calculated end-methyl to methylene CH_3/CH_2 ($R_{3/2}$) ratios suggest significant diversity in mat-builders from different horizons, however, all ratios fall within the range of extant prokaryotes (Fig. 8A; Table 3). In the Josefsdal Chert, $R_{3/2}$ ratios varying between 0.195 and 0.769, with 25th and 75th percentiles of 0.337 and 0.568, respectively, are consistent with both bacterial and archaeal origins (Igisu *et al.* 2009, 2018), however, the many low values below 0.4 necessitate a strong input from bacterial membrane lipids. Although higher values between 0.45 and 0.75 are consistent with archaeal lipid origins (Atlas 1989; Igisu *et al.* 2012) and thus suggest a mixed ecosystem, we nonetheless find that the Josefsdal Chert mats were bacterially dominated. Mats of the Footbridge Chert tell a similar story: $R_{3/2}$ ratios between 0.337 and 0.796 (with one outlier at 1.270), with 25th and 75th percentiles at 0.426 and 0.754 respectively, are consistent with mixed bacterial and archaeal origins. The wider distribution of points and lack of low $R_{3/2}$ ratios when compared to the Josefsdal Chert suggest that at least some carbonaceous material is derived from archaeal membrane lipids; however, a concentration of points around 0.6–0.7 also indicates a bacterial cellular signal. In the Hooggenoeg Chert samples, the limited range of low $R_{3/2}$ ratios of between 0.184 and 0.506, is consistent with a signal dominated by bacterial membrane lipids. Finally, the Middle Marker horizon shows a distribution unlike the other three formations, with higher $R_{3/2}$ ratios between 0.779 and 1.249, and 25th and 75th percentiles at 0.824 and 1.023 respectively, potentially diagnostic of a near-pure archaeal consortium. Although the $R_{3/2}$ ratio may not necessarily be applicable to archaeal material (due to the fact that the highly simplified *n*-alkane model of Lin & Ritz (1993) upon which it is based has no direct link to isoprenoids) the $R_{3/2}$ values for the Middle Marker chert mats are inconsistent with bacterial membrane lipid origins. In the absence of other logical solutions, we follow the extrapolation of the *n*-alkane model by Igisu *et al.* (2009), who suggested that the $R_{3/2}$ ratio of archaeal lipids would average 1.16, not dissimilar to our own measurements in mats from the Middle Marker horizon. Nonetheless, measurements of archaeal lipids by Igisu *et al.* (2012) found that values could be lower ($R_{3/2}$ = 0.50–0.75), while archaeal cells had much higher values ($R_{3/2}$ = 0.75–1.10). We therefore suggest a strong contribution from archaeal cell material in the Middle Marker mats. The outlier point ($R_{3/2}$ = 1.270) in the Footbridge Chert mats may also reflect an archaeal cell contribution, perhaps evidencing within-mat heterogeneity. This is supported by the concentration of elevated $R_{3/2}$ ratios in Footbridge Chert material relative to the conspicuously bacterially dominated Hooggenoeg and Josefsdal cherts. PCA (Fig. 10), scatter plots (Fig. 9A–C) and ANOVA of coupled to the

Tukey's and REGWQ tests (Table 2) all note a higher degree of similarity between $R_{3/2}$ in the Footbridge Chert and Middle Marker mats than between any other samples and the Middle Marker mats. We thus suggest that the Footbridge Chert mats were home to a well-mixed bacterial–archaeal consortium.

Palaeoarchaean mats thus reflect diverse microbial consortia in which Bacteria and Archaea flourished alongside one another in shallow-water anoxygenic environments (Fig. 11; Table 3). The Middle Marker mats may reflect an unusual, uniquely archaeal system. Convincing fossil evidence for Archaea is extremely rare and primarily consists of either very negative carbon isotopes consistent with the archaeal clade conducting anaerobic oxidation of methane (Ueno *et al.* 2006) or Fe and Ni-enriched carbonaceous materials that may preserve co-factors from the palaeometallome of archaeal biomass (Hickman-Lewis *et al.* 2020*b*). Alternatively, and in accordance with the lower intensity of FTIR spectral characteristics in the Middle Marker horizon, the difference in Bacteria-dominated and Archaea-dominated systems may indicate that while Bacteria were the most common primary producers, Archaea were the most common heterotrophic degraders, and the Middle Marker mats have simply undergone further degradation prior to silicification; i.e. their silicification was less rapid. This alternative, however, rests on the assumption that the relative microbial compositions of producer and degrader niches have been constant through time.

We have thus demonstrated, for the first time, unequivocal distinctions between the bacterial and archaeal communities constructing microbial mats in Earth's early ecosystems and have shown that taxonomic specificity may be preserved in FTIR spectra for more than 3 Gyr.

Rapid silicification allows exceptional preservation of FTIR signatures

FTIR spectral features diagnostic of the precursor materials, for example the CH_3/CH_2 ratio, may be preserved through diagenesis and catagenesis (Peters *et al.* 2005; Igisu *et al.* 2006, 2018; Guido *et al.* 2013; Hackley *et al.* 2017). Post-mortem biological reworking combined with deep burial at depths greater than 3 km and temperatures higher than 250°C, however, appear to cause diagenetic modification of IR bio-indicators (Peters *et al.* 2005; Lis *et al.* 2005; Fraser *et al.* 2014). The samples studied herein have undergone lower greenschist metamorphism (~3–4 kbar, 285–400°C) i.e. alteration higher than that presupposing the preservation of IR spectral heterogeneity. In spite of this, we have unambiguously demonstrated that variance in FTIR spectra is due to biomolecular diversity in the original biomass. Furthermore, there is no evidence for post-diagenetic biological recombination of the carbonaceous materials within samples, which were obtained from clean, unweathered cherts free of textural or chemical alteration. This inconsistency requires explanation. Why, contrary to expectations, do the carbonaceous materials within these cherts preserve primary bio-indicative signals?

We suggest that silicification, which was suggested to be early and rapid in Palaeoarchaean cherts due to the elevated concentrations of Si in the oceans of the time

TABLE 3. Summary of measured parameters from FTIR spectra with inferences made regarding the composition of relic biopolymers and the architect microbial community, reflecting the community composition of the mats at the time of fossilization.

Unit	Sample	CH_3/CH_2 ($R_{3/2}$)	Biological community	CH_2/CH_3	*n*-alkane chain length (approx.)	Aliphatic/ aromatic
Middle Marker	07SA21	0.785–0.994	Archaea-dominated	1.033–1.284	5–6	0.014–0.047
	07SA23	0.811–1.249	Archaea-dominated	0.813–1.233	5–6	0.008–0.053
Hooggenoeg Chert H5c	03SA15	0.287–0.506	Bacteria-dominated	1.975–3.593	7–10	0.032–0.066
	03SA15B	0.184–0.370	Bacteria-dominated	2.706–5.447	9–13	0.024–0.046
Footbridge Chert	03SA09	0.377–0.796 (outlier discounted)	Mixed community	0.787–2.652	5–9	0.024–0.048
Josefsdal Chert	12SA18	0.195–0.769	Mixed community	1.300–3.044 (outlier discounted)	6–9	0.019–0.042
	12SA36	0.364–0.586	Mixed community	1.706–2.750	7–9	0.024–0.037

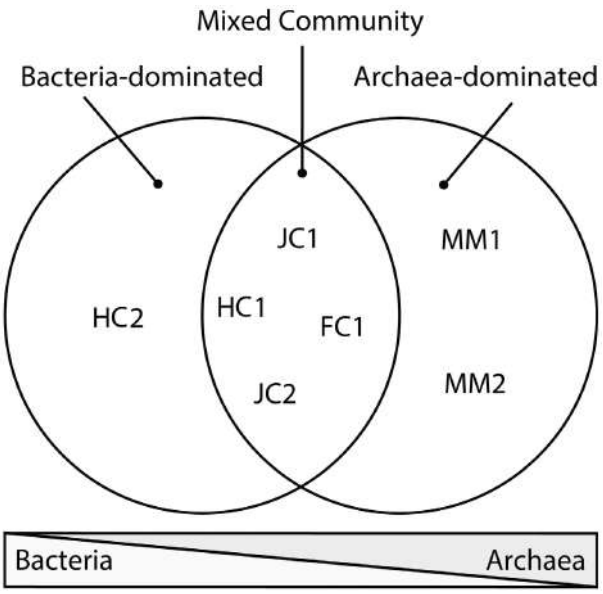

FIG. 11. Venn diagram qualitatively summarizing the results of all measurements and statistical analyses. Samples can clearly be categorized along a shifting scale from bacterial to archaeal ecosystem dominance. Most microbial mats comprised a variably mixed community.

(Maliva *et al.* 2005; Westall *et al.* 2015; Alleon *et al.* 2016*a*; Hickman-Lewis *et al.* 2020*a*) inhibits the alteration of even fine-scale biomolecular heterogeneity in organic material. Microbes can also mediate their own silicification within extracellular polymeric substances (Moore *et al.* 2020) which, being a major component of microbial mats, may account for the exceptional diversity of biopolymers observed in these mats relative to individual microfossils in previous studies. This corroborates previous experimental determination that early diagenetic silicification preserves relics of original biomolecular composition at up to zeolite facies (150–170°C; Alleon *et al.* 2016*a*) and even as far as sub-greenschist facies (250°C and 250 bars; Alleon *et al.* 2016*b*). We here propose that, when the silicification of biomass is exceptionally rapid, as was the case for these rocks, biochemical moieties reflecting palaeobiology may endure through even lower greenschist metamorphism. Furthermore, since silicification began during the life cycle of the organisms building these microbial mats, hence the volumetric preservation of biofilms, (Walsh & Lowe 1999; Walsh & Westall 2003; Hickman-Lewis *et al.* 2018*a*) and three-dimensional preservation of micromorphologies within (Hickman-Lewis *et al.* 2017, 2019), the IR signal preserved is that of the architect mat-building community at the moment of silicification. Differentiating between the IR signals preserved in microbial mats of various morphologies and within various palaeoenvironmental settings could aid both in constraining their original biological communities and in the eventual reconstruction of the biomes of Archaean life of which they were a part.

CONCLUSIONS

Palaeoarchaean surface productivity was distributed throughout systems of basins teeming with microbial life, the fragmentary records of which are preserved in greenstone belts. Constraining the microbial communities within is one of the principal outstanding challenges facing Archaean palaeontology.

Applying FTIR spectroscopy to multiple microbial mat horizons from the Palaeoarchaean of the Barberton greenstone belt, we have demonstrated that spectral characteristics can delineate relics of the biopolymer compositions of their architect anoxygenic photosynthetic communities and, more critically, the relative proportions of the domains of life in these mats. The range of biomolecular relics preserved in these mats is considerably greater than in individual microfossils and reflects the organic composition of original biomass, i.e. cells and extracellular products. Using the CH_3/CH_2 and CH_2/CH_3 ratios, together with qualitative assessments of absorption band intensity, we have quantitatively compared the architect communities of four horizons (the 3.472 Ga Middle Marker, 3.45 Ga Hooggenoeg Chert H5c, 3.334 Ga Footbridge Chert and the 3.33 Ga Josefsdal Chert) and shown statistically significant differences between them. Whereas mats of the Middle Marker horizon appear to reflect dominantly archaeal communities, the Hooggenoeg mats result from dominantly bacterial sources. The Josefsdal mats, some Hooggenoeg mats and, especially, the Footbridge mats were built by mixed consortia, indicated by wider ranges of CH_3/CH_2 and CH_2/CH_3 ratios, which show evidence for bacterial and archaeal precursor material.

Such exceptional preservation of biomolecular relics is largely inconsistent with the lower greenschist metamorphism experienced by these rocks. The retention of spectral characteristics demands almost immediate syndepositional preservation, which is consistent with early, rapid silicification of these horizons. Chertified fossiliferous horizons provide an unparalleled window on the primitive biosphere and serve as palaeobiological testament to the diversity of Archaean microbial ecosystems. We suggest that Bacteria and Archaea were already flourishing together in these ecosystems by 3.5 Ga.

Acknowledgements. This work was funded by the INACMa (Inorganic Nanoparticles in Archaean Carbonaceous Matter – a key to early life and palaeoenvironmental reconstructions) project (EU-FP7 Grant no. 618657) to BC. FTIR analyses were conducted with Fabio Bergamini (Centro Interdipartimentale Grandi Strumenti, Modena, Italy). We thank Assimo Maris

(Università di Bologna), for valuable comments on the statistical analyses and Sylvain Janiec (Institut des Sciences de la Terre d'Orléans, France) for producing all thin sections. Four reviewers provided many helpful comments and suggestions that led to significant improvement of the paper.

Author contributions. KHL and BC conceived the research. FW collected the samples. KHL performed the experiments and analysed the data. All authors contributed to discussion of the data. KHL wrote the paper, to which all authors contributed.

DATA ARCHIVING STATEMENT

FTIR Data for this study are archived at the Centre National de la Recherche Scientifique, France, and are available from the Dryad Digital Repository: https://doi.org/10.5061/dryad.v41ns1rsn

Editor. Barry Lomax

REFERENCES

ALBERS, S. V. and MEYER, B. H. 2011. The archaeal cell envelope. *Nature Reviews Microbiology*, **9**, 414–426.

ALLEON, J., BERNARD, S., LE GUILLOU, C., MARIN-CARBONNE, J., PONT, S., BEYSSAC, O., MCKEEGAN, K. D. and ROBERT, F. 2016*a*. Molecular preservation of 1.88 Ga Gunflint organic microfossils as a function of temperature and mineralogy. *Nature Communications*, **7**, 11977.

—— —— —— DAVAL, D., SKOURI-PANET, F., PONT, S., DELBES, L. and ROBERT, F. 2016*b*. Early entombment within silica minimizes the molecular degradation of microorganisms during advanced diagenesis. *Chemical Geology*, **437**, 98–108.

AROURI, K., GREENWOOD, P. F. and WALTER, M. R. 1999. A possible chlorophycean affinity of some Neoproterozoic acritarchs. *Organic Geochemistry*, **30**, 1323–1337.

ATLAS, R. M. (ed.) 1989. *Microbiology: Fundamentals and applications*. Macmillan.

AWRAMIK, S. M. and BARGHOORN, E. S. 1977. The Gunflint microbiota. *Precambrian Research*, **5**, 121–142.

BARGHOORN, E. S. and TYLER, S. A. 1965. Microorganisms from the Gunflint Chert. *Science*, **147**, 563–575.

BELLAMY, L. J. 1954. *The infra-red spectra of complex molecules*. John Wiley & Sons.

BENNING, L. G., PHOENIX, V. R., YEE, N. and TOBIN, M. J. 2004. Molecular characterization of cyanobacterial silicification using synchrotron infrared micro-spectroscopy. *Geochimica et Cosmochimica Acta*, **68**, 729–741.

BONNEVILLE, S., DELPOMDOR, F., PRÉAT, A., CHEVALIER, C., ARAKI, T., KAZEMIAN, M., STEELE, A., SCHREIBER, A., WIRTH, R. and BENNING, L. G. 2020. Molecular identification of fungi microfossils in a Neoproterozoic shale rock. *Science Advances*, **22**, eaax7599.

BOSAK, T., GREENE, S. and NEWMAN, D. K. 2007. A likely role for anoxygenic photosynthetic microbes in the formation of ancient stromatolites. *Geobiology*, **5**, 119–126.

—— BUSH, J. W. M., FLYNN, M. R., LIANG, B., ONO, S., PETROFF, A. P. and SIM, M. S. 2010. Formation and stability of oxygen-rich bubbles that shape photosynthetic mats. *Geobiology*, **8**, 45–55.

BYERLY, G. R., LOWE, D. R. and HEUBECK, C. 2018. Geologic evolution of the Barberton greenstone belt – a unique record of crustal development, surface processes, and early life. 3.55–3.20 Ga. 569–613. *In* VAN KRANENDONK, M. J., BENNETT, V. C. and HOFMANN, J. E. (eds) *Earth's oldest rocks*. 2nd edn. Elsevier.

CHEN, Y., ZOU, C., MASTALERZ, M., HU, S., GASAWAY, C. and TAO, X. 2015. Applications of micro-Fourier Transform Infrared Spectroscopy (FTIR) in the geological sciences—a review. *International Journal of Molecular Sciences*, **16**, 30223–30250.

CHOO-SMITH, L. Q., MAQUELIN, K., VAN VREESWIJK, T., BRUINING, H. A., PUPPELS, G. J., THI, N., KIRSCHNER, C., NAUMANN, D., AMI, D., VILLA, A. M., ORSINI, F., DOGLIA, S. M., LAMFARRAJ, H. and SOCKALINGUM, G. D. 2001. Investigating microbial (micro)colony heterogeneity by vibrational spectroscopy. *Applied & Environmental Microbiology*, **67**, 1461–1469.

DE LEEUW, J. W., VERSTEEGH, G. J. M. and VAN BERGEN, P. F. 2006. Biomacromolecules of algae and plants and their fossil analogues. *Plant Ecology*, **182**, 209–233.

DERENNE, S., ROBERT, F. and SKRZYPCZAK-BONDUELLE, A. 2008. Molecular evidence for life in the 3.5 billion year old Warrawoona chert. *Earth & Planetary Science Letters*, **272**, 476–480.

FRASER, W. T., SCOTT, A. C., FORBES, A. E. S., GLASSPOOL, I. J., PLOTNICK, R. E., KENIG, F. and LOMAX, B. H. 2012. Evolutionary stasis of sporopollenin biochemistry revealed by unaltered Pennsylvanian spores. *New Phytologist*, **196**, 397–401.

—— WATSON, J. S., SEPHTON, M. A., LOMAX, B. H., HARRINGTON, G., GOSLING, W. D. and SELF, S. 2014. Changes in spore chemistry and appearance with increasing maturity. *Review of Palaeobotany & Palynology*, **201**, 41–46.

GUIDO, A., MASTANDREA, A., TOSTI, F., DEMASI, F., BLANCO, A., D'ELIA, M., OROFINO, V., FONTI, S. and RUSSO, F. 2012. Characterization of fossil organic matter with Fourier-Transform Infrared (FTIR) Spectroscopy: an attempt to record extraterrestrial life. *Memorie Della Società Astronomica Italiana Supplementi*, **20**, 64.

—— —— and RUSSO F. 2013. Biotic vs abiotic carbonates: characterisation of the fossil organic matter with Fourier-Transform Infrared (FT-IR) spectroscopy. *Bollettino Della Società Paleontologica Italiana*, **52**, 63–70.

GUPTA, N. S., BRIGGS, D. E. G., COLLINSON, M. E., EVERSHED, R. P., MICHELS, R. and PANCOST, R. D. 2007. Molecular preservation of plant and insect cuticles from the Oligocene Enspel Formation, Germany: evidence against derivation of aliphatic polymer from sediment. *Organic Geochemistry*, **38**, 404–418.

HACKLEY, P. C., WALTERS, C. C., KELEMEN, S. R., MASTALERZ, M. and LOWERS, H. A. 2017. Organic petrology and micro-spectroscopy of *Tasmanites* microfossils:

applications to kerogen transformations in the early oil window. *Organic Geochemistry*, **114**, 23–44.

HELM, D. and NAUMANN, D. 1995. Identification of some bacterial cell components by FT-IR spectroscopy. *FEMS Microbiology Letters*, **126**, 75–79.

HICKMAN-LEWIS, K., GARWOOD, R.J., WITHERS, P.J. and WACEY, D. 2017. X-ray microtomography as a tool for investigating the petrological context of Precambrian cellular remains. 33–56. *In* BRASIER, A. T., MCILROY, D. and MCLOUGHLIN, N. (eds) *Earth system evolution and early life: A celebration of the work of Martin Brasier*. Geological Society of London Special Publications, **448**.

—— CAVALAZZI, B., FOUCHER, F. and WESTALL, F. 2018*a*. Most ancient evidence for life in the Barberton Greenstone Belt: microbial mats and biofabrics of the ~3.47 Ga middle marker horizon. *Precambrian Research*, **312**, 45–67.

—— WESTALL, F. and CAVALAZZI, B. 2018*b*. Traces of early life from the Barberton greenstone belt. 1029–1058. *In* VAN KRANENDONK, M. J., BENNETT, V. C. and HOFMANN, J. E. (eds) *Earth's oldest rocks*. 2nd edn. Elsevier.

—— GAUTRET, P., ARBARET, L., SORIEUL, S., DE WIT, R., FOUCHER, F., CAVALAZZI, B. and WESTALL, F. 2019. Mechanistic morphogenesis of organo-sedimentary structures growing under geochemically stressed conditions: keystone to the interpretation of some Archaean stromatolites? *Geosciences*, **9**, 359.

—— GOURCEROL, B., WESTALL, F., MANZINI, D. and CAVALAZZI, B. 2020*a*. Reconstructing Palaeoarchaean microbial biomes flourishing in the presence of emergent landmasses using trace and rare earth element systematic. *Precambrian Research*, **342**, 105689.

—— CAVALAZZI, B., SORIEUL, S., GAUTRET, P., FOUCHER, F., WHITEHOUSE, M. J., JEON, H., COCKELL, C. S., GEORGELIN, T. and WESTALL, F. 2020*b*. Metallomics in deep time and the influence of ocean chemistry on the metabolic landscapes of Earth's earliest ecosystems. *Scientific Reports*, **10**, 4965.

—— WESTALL, F. and CAVALAZZI, B. 2020*c*. Data from: Diverse communities of bacteria and archaea flourished in Palaeoarchaean (3.5–3.3 Ga) microbial mats. *Dryad Digital Repository*. https://doi.org/10.5061/dryad.v41ns1rsn

HOMANN, M., HEUBECK, C., AIRO, A. and TICE, M. M. 2015. Morphological adaptations of 3.22 Ga-old tufted microbial mats to Archean coastal habitats (Moodies Group, Barberton Greenstone Belt, South Africa). *Precambrian Research*, **266**, 47–64.

—— SANSJOFRE, P., VAN ZUILEN, M., HEUBECK, C., GONG, J., KILLINGSWORTH, B., FOSTER, I. S., AIRO, A., VAN KRANENDONK, M. J., ADER, M. and LALONDE, S. V. 2018. Microbial life and biogeochemical cycling on land 3,220 million years ago. *Nature Geoscience*, **11**, 665–671.

IGISU, M., NAKASHIMA, S., UENO, Y., AWRAMIK, S. M. and MARUYAMA, S. 2006. In situ infrared microspectroscopy of ~850 million-year-old prokaryotic fossils. *Applied Spectroscopy*, **60**, 1111–1120.

—— UENO, Y., SHIMOJIMA, M., NAKASHIMA, S., AWRAMIK, S. M., OHTA, H. and MARUYAMA, S. 2009. Micro-FTIR signature of bacterial lipids in proterozoic microfossils. *Precambrian Research*, **173**, 19–26.

—— TAKAI, K., UENO, Y., NISHIZAWA, M., NUNOURA, T., HIRAI, M., KANEKO, M., NARAOKA, H., SHIMOJIMA, M., HORI, K., NAKASHIMA, S., OHTA, H., MARUYAMA, S. and ISOZAKI, Y. 2012. Domain-level identification and quantification of relative prokaryotic cell abundance in microbial communities by micro-FTIR spectroscopy. *Environmental Microbiology Reports*, **4**, 42–49.

—— UENO, Y. and TAKAI, K. 2018. FTIR microspectroscopy of carbonaceous matter in ~ 3.5 Ga seafloor hydrothermal deposits in the North Pole area, Western Australia. *Progress in Earth & Planetary Science*, **5**, 85.

—— KOMIYA, T., AWRAMIK, S. M., IKEMOTO, Y., GENG, Y., UEHARA, H. and TAKAI, K. 2019. Fourier transform infrared microspectroscopic characterization of Neoproterozoic organic microfossils from the Fifteenmile Group in Yukon, Canada. *Island Arc*, **28**, e12310.

JARDINE, P. E., FRASER, W. T., LOMAX, B. H. and GOSLING, W. D. 2015. The impact of oxidation on spore and pollen chemistry. *Journal of Micropalaeontology*, **34**, 139–149.

JAVAUX, E. J. and MARSHALL, C. P. 2006. A new approach in deciphering early protist paleobiology and evolution: combined microscopy and microchemistry of single Proterozoic acritarchs. *Review of Palaeobotany & Palynology*, **139**, 1–15.

KODNER, R. B., SUMMONS, R. E. and KNOLL, A. H. 2009. Phylogenetic investigation of the aliphatic, non-hydrolyzable biopolymer algaenan, with a focus on green algae. *Organic Geochemistry*, **40**, 854–862.

LIN, R. and RITZ, G. P. 1993. Studying individual macerals using i.r. microspectroscopy, and implications on oil versus gas/condensate proneness and low rank generation. *Organic Geochemistry*, **20**, 695–706.

LIS, G. P., MASTALERZ, M., SCHIMMELMANN, A., LEWAN, M. D. and STANKIEWICZ, B. A. 2005. FTIR absorption indices for thermal maturity in comparison with vitrinite reflectance R_0 in type-II kerogens from Devonian black shales. *Organic Geochemistry*, **36**, 1533–1552.

MALIVA, R. G., KNOLL, A. H. and SIMONSON, B. M. 2005. Secular change in the Precambrian silica cycle: insights from chert petrology. *Geological Society of America Bulletin*, **117**, 835–845.

MARSHALL, C. P., JAVAUX, E. J., KNOLL, A. H. and WALTER, M. R. 2005. Combined micro-Fourier transform infrared (FTIR) spectroscopy and micro-Raman spectroscopy of Proterozoic acritarchs: a new approach to palaeobiology. *Precambrian Research*, **138**, 208–224.

—— LOVE, G. D., SNAPE, C. E., HILL, A. C., ALLWOOD, A. C., WALTER, M. R., VAN KRANENDONK, M. J., BOWDEN, S. A., SYLVA, S. P. and SUMMONS, R. E. 2007. Structural characterization of kerogen in 3.4 Ga Archaean cherts from the Pilbara Craton, Western Australia. *Precambrian Research*, **155**, 1–23.

—— EDWARDS, H. G. M. and JEHLICKA, J. 2010. Understanding the application of Raman spectroscopy to the detection of traces of life. *Astrobiology*, **10**, 229–243.

MOORE, K. R., PAJUSALU, M., GONG, J., SOJO, V., MATREUX, T., BRAUN, D. and BOSAK, T. 2020. Biologically mediated silicification of marine cyanobacteria and implications for the Proterozoic fossil record. *Geology*, published online 29 May. https://doi.org/10.1130/g47394.1

NAUMANN, D., HELM, D. and LABISCHINSKI, H. 1991. Microbiological characterizations by FT-IR spectroscopy. *Nature*, **351**, 81–82.

—— SCHULTZ, C. and HELM, D. 1996. What can infrared spectroscopy tell us about the structure and composition of intact bacterial cells? 279–310. *In* MANTSCH, H. H. and CHAPMAN, D. (eds) *Infrared spectroscopy of biomolecules*. Wiley-Liss.

NISBET, E. G. and FOWLER, C. M. R. 1999. Archaean metabolic evolution of microbial mats. *Proceedings of the Royal Society B*, **266**, 2375–2382.

NOFFKE, N. 2010. *Microbial mats in sandy deposits from the Archean Era to today*. Springer, 175 pp.

—— CHRISTIAN, D., WACEY, D. and HAZEN, R. M. 2013. Microbially induced sedimentary structures recording an ancient ecosystem in the ca. 3.48 billion-year-old Dresser Formation, Pilbara, Western Australia. *Astrobiology*, **13**, 1103–1124.

OLCOTT MARSHALL, A. and MARSHALL, C. P. 2015. Vibrational spectroscopy of fossils. *Palaeontology*, **58**, 201–211.

PAINTER, P. C., STARSINIC, M. and COLEMAN, M. M. 1985. Determination of functional groups in coal by Fourier transform interferometry. 169–240. *In* FERRARO, J. R. and BASILE, L. J. (eds) *Fourier transform infrared spectroscopy. Vol. 4*. Academic Press.

PETERS, K. E., WALTERS, C. C. and MOLDOWAN, J. M. 2005. *The biomarker guide*. Vol. 2. Cambridge University Press, 1155 pp.

QU, Y., ENGDAHL, A., ZHU, S., VAJDA, V. and McLOUGHLIN, N. 2015. Ultrastructural heterogeneity of carbonaceous material in ancient cherts: investigating biosignature origin and preservation. *Astrobiology*, **15**, 825–842.

SCHOPF, J. W. and BLACIC, J. M. 1971. New microorganisms form the Bitter Springs formation (late Precambrian) of the north-central Amadeus Basin, Australia. *Journal of Paleontology*, **45**, 925–960.

SOCRATES, G. 1980. *Infrared and Raman characteristic group frequencies*. John Wiley & Sons, 366 pp.

STEEMANS, P., LEPOT, K., MARSHALL, C. P., LE HERISSE, A. and JAVAUX, E. J. 2010. FTIR characterisation of the chemical composition of Silurian miospores (cryptospore and trilete spores) from Gotland, Sweden. *Review of Palaeobotany & Palynology*, **162**, 577–590.

TICE, M. M. 2009. Environmental controls on photosynthetic microbial mat distribution on and morphogenesis on a 3.42 Ga clastic-starved platform. *Astrobiology*, **9**, 989–1000.

—— and LOWE, D. R. 2006. The origin of carbonaceous matter in pre-3.0 Ga greenstone terrains: a review and new evidence from the 3.42 Ga Buck Reef Chert. *Earth-Science Reviews*, **76**, 259–300.

—— BOSTICK, B. C. and LOWE, D. R. 2004. Thermal history of the 3.5–3.2 Ga Onverwacht and Fig Tree Groups, Barberton greenstone belt, South Africa, inferred by Raman microspectroscopy of carbonaceous material. *Geology*, **32**, 37–40.

TROWER, E. J. and LOWE, D. R. 2016. Sedimentology of the <3.3 Ga upper Mendon Formation, Barberton greenstone belt, South Africa. *Precambrian Research*, **281**, 473–494.

UENO, Y., YAMADA, K., YOSHIDA, N., MARUYAMA, S. and ISOZAKI, Y. 2006. Evidence from fluid inclusions for microbial methanogenesis in the early Archaean era. *Nature*, **440**, 516–519.

VERSTEEGH, G. J. M. and BLOKKER, P. 2004. Resistant macromolecules of extant and fossil microalgae. *Phycological Research*, **52**, 325–339.

WACEY, D., BATTISON, L., GARWOOD, R. J., HICKMAN-LEWIS, K. and BRASIER, M. D. 2017. Advanced analytical techniques for studying the morphology and chemistry of Proterozoic microfossils. 81–104. *In* BRASIER, A. T., McILROY, D. and McLOUGHLIN, N. (eds) *Earth system evolution and early life: A celebration of the work of Martin Brasier*. Geological Society of London Special Publications, **448**.

WALSH, M. M. and LOWE, D. R. 1999. Modes of accumulation of carbonaceous matter in the early Archaean: a petrographic and geochemical study of the carbonaceous cherts of the Swaziland Supergroup. 115–132. *In* LOWE, D. R. and BYERLY, G. R. (eds) *Geologic evolution of the Barberton Greenstone Belt, South Africa*. Geological Society of America Special Paper, **329**.

—— and WESTALL, F. 2003. Archean biofilms preserved in the Swaziland supergroup, South Africa. 307–316. *In* KRUMBEIN, W. E., PATERSON, D. M. and ZAVARZIN, G. A. (eds) *Fossil and recent biofilms: A natural history of life on earth*. Kluwer.

WESTALL, F., CAVALAZZI, B., LEMELLE, L., MARROCCHI, Y., ROUZAUD, J. N., SIMIONOVICI, A., SALOMÉ, M., MOSTEFAOUI, S., ANDREAZZA, C., FOUCHER, F., TOPORSKI, J., JAUSS, A., THIEL, V., SOUTHAM, G., MACLEAN, L., WIRICK, S., HOFMANN, A., MEIBOM, A., ROBERT, F. and DÉFARGE, C. 2011. Implications of in situ calcification for photosynthesis in a <3.3 Ga-old microbial biofilm from the Barberton Greenstone Belt, South Africa. *Earth & Planetary Science Letters*, **310**, 468–479.

—— CAMPBELL, K. A., BRÉHÉRET, J. G., FOUCHER, F., GAUTRET, P., HUBERT, A., SORIEUL, S., GRASSINEAU, N. and GUIDO, D. M. 2015. Archean (3.33 Ga) microbe-sediment systems were diverse and flourished in a hydrothermal context. *Geology*, **43**, 615–618.

XIE, X., BYERLY, G. R. and FERRELL, R. E. Jr 1997. IIb trioctahedral chlorite from the Barberton greenstone belt: crystal structure and rock composition constraints with implications to geothermometry. *Contributions to Mineralogy & Petrology*, **126**, 275–291.

YEE, N., BENNING, L. G., PHOENIX, V. R. and FERRIS, F. G. 2004. Characterization of metal-cyanobacteria sorption reactions: a combined macroscopic and infrared spectroscopic investigation. *Environmental Science & Technology*, **38**, 775–782.